International Journal of Solids and Structures 46 (2009) 3710–3724

Contents lists available at ScienceDirect

International Journal of Solids and Structures

journal homepage: www.elsevier.com/locate/ijsolstr

Investigation of mixed-mode stress intensity factors for nonhomogeneous materials using an interaction integral method

Hongjun Yu *, Linzhi Wu *, Licheng Guo, Shanyi Du, Qilin He

Center for Composite Materials, Harbin Institute of Technology, Harbin 150001, China

ARTICLE INFO

Article history:
Received 18 January 2009
Received in revised form 23 May 2009
Available online 30 June 2009

Keywords:
Interaction (energy) integral
Stress intensity factors (SIFs)
Extended finite element method (XFEM)
Nonhomogeneous materials

ABSTRACT

An interaction (energy) integral is derived for the computation of mixed-mode stress intensity factors (SIFs) in nonhomogeneous materials with continuous or discontinuous properties. This method is based on a conservation integral that relies on two admissible mechanical states (actual and auxiliary fields). In general, the interaction energy contour integral is converted into an equivalent domain integral in numerical computations. It can be seen from the equivalent domain integral, the integrand does not involve any derivatives of material properties. Moreover, the formulation can be proved valid even when the integral domain contains material interfaces. Therefore, it is not necessary to limit the material properties to be continuous for the present method. Due to these advantages the application range of the interaction integral method can be greatly enlarged. The numerical implementation of the derived expression is combined with the extended finite element method (XFEM). Using this method, the influences of material properties on the mixed-mode SIFs are investigated for four types of material properties selected in this work. Numerical results show that the mechanical properties and their first-order derivatives can affect mode I and II SIFs greatly, while the higher-order derivatives affect the SIFs very slightly.

1. Introduction

Composite materials have been applied in many fields to withstand highly severe conditions such as aircraft fuselages and chemical activators. Recently, many composite materials and structures have been designed and produced with nonhomogeneous properties. Fracture is a common failure mode for those nonhomogeneous materials and structures in service, and the numerical technique is one of the most convenient and reliable methods to determine the fracture parameters.

Among the available numerical methods, J contour integral (Rice, 1968) has generated a great interest for its convenience in solving the parameters characterizing crack-tip fields. The contour integral has been proved to be a conservation integral for homogeneous materials. The contour integrals and their associated domain formulations have been investigated by Moran and Shih (1987a,b). Eischen (1987) proved that for nonhomogeneous materials with continuous and generally differentiable properties, the stress and strain singularity near a crack tip is identical as the well-known inverse square root stress singularity in homogeneous materials. Subsequently, a modified integral J_1^* (Eischen, 1987) and a path-independent J_e-integral (Honein and Herrmann, 1997) were introduced for nonhomogeneous materials. Jin and Sun (2007) provided a mathematically rigorous proof that for nonhomogeneous materials, both J_1^* and J_e are the (potential) energy release rates. Rice (1988) and Hutchinson and Suo (1992) conducted a lot of investigations on the interface crack, and Smelser and Gurtin (1977) proved J-integral to be still path-independent for a straight interface crack.

In order to obtain mode I and mode II stress intensity factors (SIFs) separately, an interaction (energy) contour integral method (Stern et al., 1976; Yau et al., 1980) is derived from the J-integral by considering a composition of two admissible states (the actual fields and known auxiliary fields). Wang et al. (1980) introduced this method to further study two-dimensional mixed-mode crack problems in rectilinear anisotropic solids. For the convenience of numerical calculations, Nakamura (1991) used an equivalent domain integral of the interaction integral to evaluate mixed-mode SIFs along straight three-dimensional interface cracks. The same method was employed to deal with curved three-dimensional interface crack problems (Nahta and Moran, 1993; Gosz et al., 1998). Gosz and Moran (2002) developed the interaction integral method for nonplanar three-dimensional crack problems. Subsequently, Dolbow and Gosz (2002) introduced the interaction integral method to compute mixed-mode SIFs for two-dimensional crack problems in functionally graded materials (FGMs) which are the nonhomogeneous materials with properties varying continuously. In comparison with modified J-integral for nonhomogeneous materials, they found that the interaction integral is more convenient since it does not require the evaluation of strain energy densities along the traction-free crack faces. For isotropic FGMs, Kim and Paulino (2003) computed the mixed-mode SIFs

* Corresponding authors. Tel.: +86 451 86402376; fax: +86 451 86402386.
E-mail addresses: yuhongjun@hit.edu.cn (H. Yu), wlz@hit.edu.cn (L. Wu).

0020-7683/$ - see front matter © 2009 Elsevier Ltd. All rights reserved.
doi:10.1016/j.ijsolstr.2009.06.019

and T-stress by means of the interaction integral method in combination with the finite element method (FEM). Rao and Rahman (2003) employed the method to analyze mixed-mode crack problems in orthotropic FGMs. Kim and Paulino (2005) gave a summary on three definitions of the auxiliary fields and discussed how to extract mixed-mode SIFs and T-stress for isotropic and orthotropic FGMs, respectively. Using the method, Walters et al. (2006) conducted an investigation in the mixed-mode fracture problems for three-dimensional nonhomogeneous materials. Krysl and Belytschko (1999) utilized the interaction integral method in conjunction with the element-free Galerkin method to investigate three-dimensional stationary and dynamically propagating crack problems. Song and Paulino (2006) used the approach to evaluate the dynamic SIFs for both homogeneous and nonhomogeneous materials. Johnson and Qu (2007) extended the interaction integral to calculate the SIFs of three-dimensional curvilinear cracks in a homogeneous body or on a bimaterial interface under nonuniform temperatures. KC and Kim (2008) gave the finite element evaluation of the nonsingular T-stress and mixed-mode SIFs in nonhomogeneous materials under steady-state thermal loads by the interaction integral approach. Based on full-field measurement using digital image correlation and an interaction integral, Réthoré et al. (2005) presented a technique for the experimental measurement of the SIFs under mixed-mode loading.

Most of the previous work is concerned with the materials with continuous and differentiable properties. Moreover, very few published papers have considered the influence of different types of interfaces on the SIFs. Actually, there exist more or less material interfaces in various nonhomogeneous composite materials, especially, in particulate reinforced composite materials (PRCMs). It is often found that although the PRCMs can significantly improve the strength, stiffness and wear resistance of structures (Leggoe et al., 1996), their fracture properties are not improved and, on the contrary, the fracture toughness may be significantly lower than that of the matrix material (Yang and Li, 2004). Therefore, the material interfaces have to be taken into account if the fracture performance of these composites must be concerned. In addition, FGMs have many advantages that make them attractive in potential applications, such as the improvement on residual stress distribution and mechanical durability, while in fact, FGMs are also two- or multiphase particulate composites in which material composition and microstructure vary spatially (Rahman and Chakraborty, 2007) or the volume fraction of particles varies in one or several directions (Birman and Byrd, 2007). Therefore, in certain scales, we have to investigate the material interfaces when we examine the fracture performance of FGMs.

The outline of this paper is as follows. The derivation of an interaction integral and its associated domain form without any derivatives of material properties is presented in Section 2. Section 3 gives the mathematically rigorous proof that the interaction integral method is still valid when there are material interfaces in the integral domain. Section 4 describes the method to extract the mixed-mode SIFs. Section 5 describes an extended finite element method (XFEM) and then, the numerical discretization of the interaction integral is given. Section 6 presents several numerical examples. First, two fracture problems are analyzed to verify the accuracy of the numerical method. Then, the convergence of the XFEM and the interaction integral is investigated. Next, we study the influence of material continuity on the SIFs by selecting four types of material properties. Finally, a summary and some conclusions are provided in Section 7.

2. Interaction integral

In this section, we will derive the interaction integral for extracting mixed-mode SIFs at the crack tips. Throughout this work, our attention is restricted to plane problems, the material is limited to linear-elastic and small strain kinematics is assumed.

Since the interaction integral is derived from the J-integral (Rice, 1968) for two admissible states (actual and auxiliary fields), the auxiliary field is discussed first.

2.1. The auxiliary fields

To extract the mixed-mode SIFs, the auxiliary fields used in the interaction integral have several alternative choices. Here, an incompatibility formulation (Kim and Paulino, 2005) is selected and the detailed definitions (u_i^{aux}, σ_{ij}^{aux} and ε_{ij}^{aux}) are given in Appendix A.

To facilitate the following description, an extra strain field is defined as

$$\varepsilon_{ij}^{aux0} = S_{ijkl}^{tip}\sigma_{kl}^{aux} \quad (i,j,k,l = 1,2) \tag{1}$$

where S_{ijkl}^{tip} is a compliance tensor at the crack tip. As shown in Fig. 1, the indices i, j, k and l denote the components of a variable in local coordinate system originating at the crack tip. The repetition of an index in a term denotes a summation with respect to that index over its range. According to the definitions of the auxiliary fields in Appendix A, the strains ε_{ij}^{aux0} satisfy the equation

$$\varepsilon_{ij}^{aux0} = \left(u_{i,j}^{aux} + u_{j,i}^{aux}\right)/2 \tag{2}$$

where a comma denotes a partial derivative with respect to the coordinates.

2.2. Interaction energy contour integral

As shown in Fig. 1, the standard J-integral given by Rice (1968) is

$$J = \lim_{\Gamma\to 0}\int_{\Gamma}(W\delta_{1i} - \sigma_{ij}u_{j,1})n_i\,d\Gamma \tag{3}$$

where $W = \frac{1}{2}\sigma_{ij}\varepsilon_{ij} = \frac{1}{2}C_{ijkl}\varepsilon_{ij}\varepsilon_{kl} = \frac{1}{2}S_{ijkl}\sigma_{ij}\sigma_{kl}$ is the strain energy density, the symbol δ_{ij} is Kronecker delta, n_i is the unit outward normal vector to the contour Γ, and C_{ijkl} and S_{ijkl} are the stiffness and compliance tensors, respectively. When the crack faces are assumed to be traction-free, Kim and Paulino (2003) proved that

$$J = \lim_{\Gamma\to 0}\oint_{\Gamma_0}(\sigma_{ij}u_{j,1} - W\delta_{1i})m_i q\,d\Gamma \tag{4}$$

Here, $\Gamma_0 = \Gamma_1 + \Gamma^- + \Gamma_c^+ + \Gamma_c^-$, where Γ^- is the opposite integral path of Γ; m_i is the unit outward normal vector to the contour Γ_0 and therefore, $m_i = -n_i$ on Γ; q is an arbitrary weight function with values varying smoothly from 1 on Γ to 0 on Γ_1.

According to Kim and Paulino (2005), the interaction integral I, the interactional part of the superimposed load of the actual field and the auxiliary field, can be obtained

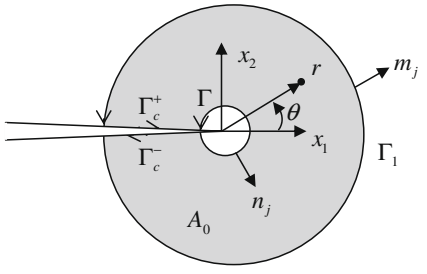

Fig. 1. Schematic illustration of the contour integrals and related equivalent domain integrals. Domain A_0 is enclosed by Γ_0 and $\Gamma_0 = \Gamma_1 + \Gamma_c^+ + \Gamma^- + \Gamma_c^-$.

$$I=\lim_{\Gamma\to 0}\oint_{\Gamma_0}\left(\sigma_{ij}^{aux}u_{j,1}+\sigma_{ij}u_{j,1}^{aux}-\frac{1}{2}\left(\sigma_{jk}^{aux}\varepsilon_{jk}+\sigma_{jk}\varepsilon_{jk}^{aux}\right)\delta_{1i}\right)m_i q\,d\Gamma \quad (5)$$

According to the definitions of the auxiliary fields in Appendix A, it can be noted that $\sigma_{ij}\varepsilon_{ij}^{aux}=C_{ijkl}(x)\varepsilon_{kl}\varepsilon_{ij}^{aux}=\sigma_{kl}^{aux}\varepsilon_{kl}$. Therefore, Eq. (5) can be simplified as

$$I=\lim_{\Gamma\to 0}\oint_{\Gamma_0}\left(\sigma_{ij}^{aux}u_{j,1}+\sigma_{ij}u_{j,1}^{aux}-\sigma_{jk}^{aux}\varepsilon_{jk}\delta_{1i}\right)m_i q\,d\Gamma \quad (6)$$

2.3. Domain form of the interaction integral

Generally, the contour integral is converted into an equivalent domain integral to avoid the potential source of inaccuracy in numerical calculations (Moran and Shih, 1987a,b). The material properties are assumed to be continuous in the domain enclosed by the contour Γ_0. Let A_0 and A denote the domains enclosed by the contours Γ_0 and Γ_1, respectively. Taking the limit $\Gamma\to 0$ leads to $A_0\to A$. By applying divergence theorem to Eq. (6), one obtains the equivalent domain integral

$$\begin{aligned}I&=\int_A\left(\sigma_{ij}^{aux}u_{j,1}+\sigma_{ij}u_{j,1}^{aux}-\sigma_{jk}^{aux}\varepsilon_{jk}\delta_{1i}\right)q_{,i}\,dA\\&\quad+\int_A\left(\sigma_{ij}^{aux}u_{j,1}+\sigma_{ij}u_{j,1}^{aux}-\sigma_{jk}^{aux}\varepsilon_{jk}\delta_{1i}\right)_{,i}q\,dA\\&=I_h+I_{nonh}\end{aligned} \quad (7)$$

The form of the first integral I_h in Eq. (7) is same as that for homogenous materials. The second term I_{nonh} can be expanded as

$$I_{nonh}=\int_A\left(\sigma_{ij,i}u_{j,1}^{aux}+\sigma_{ij,i}^{aux}u_{j,1}+\sigma_{ij}u_{j,i1}^{aux}+\sigma_{ij}^{aux}u_{j,i1}-\sigma_{ij}^{aux}\varepsilon_{ij,1}-\sigma_{ij,1}^{aux}\varepsilon_{ij}\right)q\,dA \quad (8)$$

Here, the equilibrium of stresses without body forces leads to $\sigma_{ij,i}u_{j,1}^{aux}=0$ and $\sigma_{ij,i}^{aux}u_{j,1}=0$, and the symmetry of the auxiliary stress tensor leads to $\sigma_{ij}^{aux}u_{j,i1}-\sigma_{ij}^{aux}\varepsilon_{ij,1}=0$. Hence, I_{nonh} can be simplified as

$$I_{nonh}=\int_A\left(\sigma_{ij}u_{j,i1}^{aux}-\sigma_{ij,1}^{aux}\varepsilon_{ij}\right)q\,dA \quad (9)$$

Substituting Eqs. (9) into Eq. (7), the interaction integral I can be written as

$$\begin{aligned}I&=\int_A\left(\sigma_{ij}^{aux}u_{j,1}+\sigma_{ij}u_{j,1}^{aux}-\sigma_{jk}^{aux}\varepsilon_{jk}\delta_{1i}\right)q_{,i}\,dA\\&\quad+\int_A\left(\sigma_{ij}u_{j,i1}^{aux}-\sigma_{ij,1}^{aux}\varepsilon_{ij}\right)q\,dA\end{aligned} \quad (10)$$

It should be noted that Kim and Paulino (2005) derived the same expression as Eq. (10) by assuming the material properties to be exponential functions. In this paper, it is proved that Eq. (10) is valid for the material with arbitrarily continuous properties. (Actually, it can be proved that Eq. (10) is still valid for discontinuous material properties in the following part.) Considering the symmetry of σ_{ij} and using Eqs. (1) and (2), the first integrand in Eq. (9) can be written as

$$\begin{aligned}\sigma_{ij}u_{j,i1}^{aux}&=\sigma_{ij}\frac{1}{2}(u_{j,i1}^{aux}+u_{i,j1}^{aux})=\sigma_{ij}\varepsilon_{ij,1}^{aux0}=\sigma_{ij}\left(S_{ijkl}^{tip}\sigma_{kl}^{aux}\right)_{,1}\\&=\sigma_{ij}S_{ijkl}^{tip}\sigma_{kl,1}^{aux}\end{aligned} \quad (11)$$

Substituting $\varepsilon_{ij}=S_{ijkl}(x)\sigma_{kl}$ and Eq. (11) into Eq. (10), we have

$$\begin{aligned}I&=\int_A\left(\sigma_{ij}^{aux}u_{j,1}+\sigma_{ij}u_{j,1}^{aux}-\sigma_{jk}^{aux}\varepsilon_{jk}\delta_{1i}\right)q_{,i}\,dA\\&\quad+\int_A\sigma_{ij}\left[S_{ijkl}^{tip}-S_{ijkl}(x)\right]\sigma_{kl,1}^{aux}q\,dA\end{aligned} \quad (12)$$

In order to show the advantages of Eq. (12), we will compare it with the traditional J-integral. The J-integral in the form of the stiffness can be expressed as (Dolbow and Gosz, 2002)

$$J=\int_A(\sigma_{ij}u_{j,1}-W\delta_{1i})q_{,i}\,dA-\int_A\frac{1}{2}\varepsilon_{ij}C_{ijkl,1}\varepsilon_{kl}q\,dA \quad (13)$$

It can be observed that $C_{ijkl,1}\varepsilon_{ij}\varepsilon_{kl}=\sigma_{ij,1}\varepsilon_{ij}-\varepsilon_{ij,1}\sigma_{ij}=-\sigma_{ij}S_{ijkl,1}\sigma_{kl}$ and thus, the J-integral can be expressed in the form of the compliance

$$J=\int_A(\sigma_{ij}u_{j,1}-W\delta_{1i})q_{,i}\,dA+\int_A\frac{1}{2}\sigma_{ij}S_{ijkl,1}\sigma_{kl}q\,dA \quad (14)$$

From Eqs. (13) and (14), it can be found that the derivatives of material properties ($C_{ijkl,1}$ or $S_{ijkl,1}$) exist unavoidably in the traditional J-integral. Differently, the interaction integral (Eq. (12)) does not involve any derivatives of material properties. Therefore, the interaction integral does not need the material properties to be differentiable. Since it may be difficult to obtain the derivatives of material properties or there are no derivatives in many actual cases, the applicable range of the present interaction integral is wider than that of the traditional J-integral for nonhomogeneous materials.

3. Material discontinuities (or interfaces) in the interaction integral

From the above section, it is shown that the interaction integral method does not need the nonhomogeneous material properties to be differentiable. However, the material properties are still required to be continuous in the above derivation. In this section, we will discuss whether this continuity condition of material properties is necessary in the interaction integral method.

3.1. Domain form of the interaction integral for discontinuous materials

As shown in Fig. 2, there is a bimaterial interface $\Gamma_{interface}$ in the domain enclosed by the integral contour Γ_0 and the interface is assumed to be perfectly bonded. Thus, the domain A (the domain in Γ_0 when $\Gamma\to 0$) is divided by $\Gamma_{interface}$ into two parts, i.e., A_1 and A_2 which are enclosed by the contour Γ_{01} and Γ_{02}, respectively. As a result, $A=A_1+A_2$, $\Gamma_{01}=\Gamma_{11}+\Gamma_{interface}+\Gamma_{13}+\Gamma_c^+ +\Gamma^-+\Gamma_c^-$ and $\Gamma_{02}=\Gamma_{12}+\Gamma_{interface}^-$. In this condition, Eq. (6) can be rewritten as

$$\begin{aligned}I&=\lim_{\Gamma\to 0}\oint_{\Gamma_{01}}\left(\sigma_{ij}^{aux}u_{j,1}+\sigma_{ij}u_{j,1}^{aux}-\sigma_{jk}^{aux}\varepsilon_{jk}\delta_{1i}\right)m_i q\,d\Gamma\\&\quad+\oint_{\Gamma_{02}}\left(\sigma_{ij}^{aux}u_{j,1}+\sigma_{ij}u_{j,1}^{aux}-\sigma_{jk}^{aux}\varepsilon_{jk}\delta_{1i}\right)m_i q\,d\Gamma+I_{interface}^*\end{aligned} \quad (15)$$

where $I_{interface}^*$ is a line integral along the interface with the expression shown below

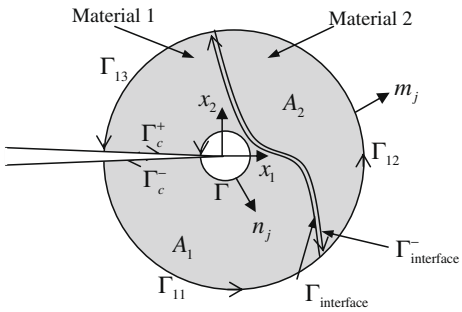

Fig. 2. An integral domain A cut by a bimaterial interface $\Gamma_{interface}$. Domains A, A_1 and A_2 are enclosed by Γ_0, Γ_{01} and Γ_{02} for $\Gamma\to 0$. Here $A=A_1+A_2$, $\Gamma_0=\Gamma_1+\Gamma^-+\Gamma_c^++\Gamma_c^-$, $\Gamma_{01}=\Gamma_{11}+\Gamma_{interface}+\Gamma_{13}+\Gamma_c^++\Gamma^-+\Gamma_c^-$ and $\Gamma_{02}=\Gamma_{12}+\Gamma_{interface}^-$.

$$I^*_{interface} = \int_{\Gamma_{interface}} \left(\sigma^{aux}_{ij} u_{j,1} + \sigma_{ij} u^{aux}_{j,1} - \sigma^{aux}_{jk}\varepsilon_{jk}\delta_{1i}\right)^{②} m_i q \, d\Gamma + \int_{\Gamma^-_{interface}} \left(\sigma^{aux}_{ij} u_{j,1} + \sigma_{ij} u^{aux}_{j,1} - \sigma^{aux}_{jk}\varepsilon_{jk}\delta_{1i}\right)^{①} m_i q \, d\Gamma \tag{16}$$

Here, the variables or expressions on the interface marked by the superscripts ① and ② means that they belong to the domains A_1 and A_2, respectively. By applying divergence theorem to the first and second integrals in Eq. (15), respectively, we have

$$I = \int_A \left(\sigma^{aux}_{ij} u_{j,1} + \sigma_{ij} u^{aux}_{j,1} - \sigma^{aux}_{jk}\varepsilon_{jk}\delta_{1i}\right) q_{,i} \, dA + \int_A \sigma_{ij}\left[S^{tip}_{ijkl} - S_{ijkl}(x)\right]\sigma^{aux}_{kl,1} q \, dA + I^*_{interface} \tag{17}$$

The value of $I^*_{interface}$ will be given in the following part.

3.2. Interface integral $I^*_{interface}$

Fig. 3(a) shows a curved bimaterial interface $\Gamma_{\text{interface}}$ with a certain distance to the crack tip. For one point p, if a point q on the interface is closest to it, the curvilinear coordinates of the point p can be defined from the following relations (Gosz and Moran, 2002)

$$\xi_1 = \mathbf{r}\cdot\mathbf{n}, \quad \xi_2 = \int_0^q dq \tag{18}$$

where $\mathbf{r}$ is the vector from q to p and $\mathbf{n}$ is the outward normal vector to $\Gamma_{\text{interface}}$ at point q. Thus, the coordinate curve ξ_1 is a straight line parallel to the vector $\mathbf{n}$. The corresponding natural base vectors $\mathbf{g}_i$ of the curvilinear coordinate system are defined by

$$\mathbf{g}_i = \frac{\partial x_k}{\partial \xi_i}\mathbf{i}_k \quad (i,k = 1,2) \tag{19}$$

where x_k are the Cartesian coordinates and $\mathbf{i}_k$ are the corresponding base vectors. If we define the angle from x_1-axis to ξ_1-axis as α, we can obtain from Eq. (18)

$$\frac{\partial \xi_1}{\partial x_1} = \cos\alpha, \quad \frac{\partial \xi_1}{\partial x_2} = \sin\alpha \tag{20}$$

For convenience, we define two orthogonal unit base vectors $\mathbf{e}_1$ and $\mathbf{e}_2$ by

$$\mathbf{e}_1 = \frac{\mathbf{g}_1}{h_1}, \quad \mathbf{e}_2 = \frac{\mathbf{g}_2}{h_2} \tag{21}$$

where $h_1 = \sqrt{\mathbf{g}_1\cdot\mathbf{g}_1}$ and $h_2 = \sqrt{\mathbf{g}_2\cdot\mathbf{g}_2}$. It is obvious from above definitions that $\mathbf{e}_1 = \mathbf{n}$ and the scale factor $h_1 = 1$ (Gosz and Moran, 2002).

According to the definitions of auxiliary fields in Appendix A, it can be observed that the auxiliary stresses and displacements and their derivatives are continuous on the interface. Therefore, $(\boldsymbol{\sigma}^{aux})^{①} = (\boldsymbol{\sigma}^{aux})^{②} = \boldsymbol{\sigma}^{aux}$ and $\left(\frac{\partial \mathbf{u}^{aux}}{\partial x_1}\right)^{①} = \left(\frac{\partial \mathbf{u}^{aux}}{\partial x_1}\right)^{②} = \frac{\partial \mathbf{u}^{aux}}{\partial x_1}$. The integral $I^*_{interface}$ in Eq. (16) can be rewritten in tensor form as

$$I^*_{interface} = \int_{\Gamma_{interface}} \left\{ \mathbf{n}\cdot\boldsymbol{\sigma}^{aux}\cdot\left[\left(\frac{\partial \mathbf{u}}{\partial x_1}\right)^{②} - \left(\frac{\partial \mathbf{u}}{\partial x_1}\right)^{①}\right] + \mathbf{n}\cdot(\boldsymbol{\sigma}^{②} - \boldsymbol{\sigma}^{①})\cdot\frac{\partial \mathbf{u}^{aux}}{\partial x_1} - \boldsymbol{\sigma}^{aux} : (\boldsymbol{\varepsilon}^{②} - \boldsymbol{\varepsilon}^{①})n_1 \right\} q \, d\Gamma \tag{22}$$

where $n_1 = \cos\alpha$ since n_1 is the component of $\mathbf{n}$ in x_1 direction as shown in Fig. 3(a). According to the equilibrium condition on the bimaterial interface, the tractions on both sides of the interface should be equal. That is

$$\boldsymbol{\sigma}^{②}\cdot\mathbf{n} = \boldsymbol{\sigma}^{①}\cdot\mathbf{n} \tag{23}$$

Since the interface is perfectly bonded, the derivatives of actual displacements with respect to the curvilinear coordinate ξ_2 are equal on both sides of the interface, i.e.,

$$\left(\frac{\partial \mathbf{u}}{\partial \xi_2}\right)^{①} = \left(\frac{\partial \mathbf{u}}{\partial \xi_2}\right)^{②} \tag{24}$$

By the chain rule we can write the first integrand in Eq. (22) in the $\xi_1 - \xi_2$ coordinate system as

$$\begin{aligned}\mathbf{n}\cdot\boldsymbol{\sigma}^{aux}\cdot\left[\left(\frac{\partial \mathbf{u}}{\partial x_1}\right)^{②} - \left(\frac{\partial \mathbf{u}}{\partial x_1}\right)^{①}\right] &= \mathbf{n}\cdot\boldsymbol{\sigma}^{aux}\cdot\left\{\left[\left(\frac{\partial \mathbf{u}}{\partial \xi_1}\right)^{②} - \left(\frac{\partial \mathbf{u}}{\partial \xi_1}\right)^{①}\right]\frac{\partial \xi_1}{\partial x_1} \right.\\ &\left. + \left[\left(\frac{\partial \mathbf{u}}{\partial \xi_2}\right)^{②} - \left(\frac{\partial \mathbf{u}}{\partial \xi_2}\right)^{①}\right]\frac{\partial \xi_2}{\partial x_1}\right\}\end{aligned} \tag{25}$$

Substituting Eqs. (20) and (24) into Eq. (25), one obtains

$$\mathbf{n}\cdot\boldsymbol{\sigma}^{aux}\cdot\left[\left(\frac{\partial \mathbf{u}}{\partial x_1}\right)^{②} - \left(\frac{\partial \mathbf{u}}{\partial x_1}\right)^{①}\right] = \mathbf{n}\cdot\boldsymbol{\sigma}^{aux}\cdot\left[\left(\frac{\partial \mathbf{u}}{\partial \xi_1}\right)^{②} - \left(\frac{\partial \mathbf{u}}{\partial \xi_1}\right)^{①}\right]\cos\alpha \tag{26}$$

According to Eq. (23), the second integrand in Eq. (22) is

$$\mathbf{n}\cdot(\boldsymbol{\sigma}^{②} - \boldsymbol{\sigma}^{①})\cdot\frac{\partial \mathbf{u}^{aux}}{\partial x_1} = 0. \tag{27}$$

In order to simplify the third integrand, applying the strain–displacement relations of actual fields, one obtains

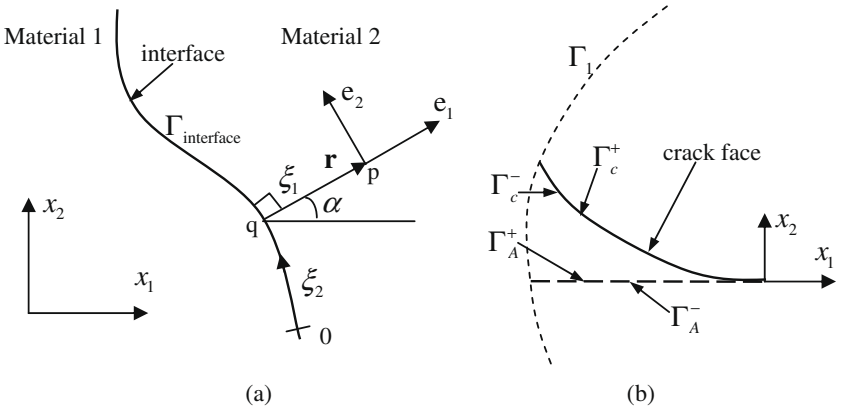

Fig. 3. A curvilinear coordinate system originating from the interface: (a) a material interface; (b) a curved crack face.

$$\boldsymbol{\sigma}^{aux}:(\boldsymbol{\varepsilon}^{②}-\boldsymbol{\varepsilon}^{①})n_1 = \boldsymbol{\sigma}^{aux}:\left[\frac{1}{2}(\nabla\mathbf{u}+\mathbf{u}\nabla)^{②}-\frac{1}{2}(\nabla\mathbf{u}+\mathbf{u}\nabla)^{①}\right]n_1 \tag{28}$$

where ∇ is the gradient operator expressed by (Gosz and Moran, 2002)

$$\nabla=\left\{\mathbf{e}_1\frac{1}{h_1}\frac{\partial}{\partial\xi_1}+\mathbf{e}_2\frac{1}{h_2}\frac{\partial}{\partial\xi_2}\right\} \tag{29}$$

Since the stress $\boldsymbol{\sigma}^{aux}$ is a symmetrical tensor, one obtains

$$\boldsymbol{\sigma}^{aux}:\mathbf{u}\nabla=(\boldsymbol{\sigma}^{aux})^T:\mathbf{u}\nabla=\boldsymbol{\sigma}^{aux}:\nabla\mathbf{u} \tag{30}$$

Substituting Eq. (30) into Eq. (28), we have

$$\boldsymbol{\sigma}^{aux}:(\boldsymbol{\varepsilon}^{②}-\boldsymbol{\varepsilon}^{①})n_1=\boldsymbol{\sigma}^{aux}:[(\nabla\mathbf{u})^{②}-(\nabla\mathbf{u})^{①}]n_1 \tag{31}$$

Substituting Eq. (29) into Eq. (31), it gives

$$\begin{aligned}\boldsymbol{\sigma}^{aux}:(\boldsymbol{\varepsilon}^{②}-\boldsymbol{\varepsilon}^{①})n_1 &= \mathbf{e}_1\cdot\boldsymbol{\sigma}^{aux}\cdot\left\{\left[\frac{\partial\mathbf{u}}{\partial\xi_1}\right]^{②}-\left[\frac{\partial\mathbf{u}}{\partial\xi_1}\right]^{①}\right\}\frac{n_1}{h_1}\\ &+\mathbf{e}_2\cdot\boldsymbol{\sigma}^{aux}\cdot\left\{\left[\frac{\partial\mathbf{u}}{\partial\xi_2}\right]^{②}-\left[\frac{\partial\mathbf{u}}{\partial\xi_2}\right]^{①}\right\}\frac{n_1}{h_2}\end{aligned} \tag{32}$$

The detailed derivations of Eq. (32) are given in Appendix B. Substituting $\mathbf{e}_1=\mathbf{n}$, $h_1=1$, $n_1=\cos\alpha$ and Eq. (24) into Eq. (32), the third integrand in Eq. (22) are finally simplified as

$$\boldsymbol{\sigma}^{aux}:(\boldsymbol{\varepsilon}^{②}-\boldsymbol{\varepsilon}^{①})n_1=\mathbf{n}\cdot\boldsymbol{\sigma}^{aux}\cdot\left[\left(\frac{\partial\mathbf{u}}{\partial\xi_1}\right)^{②}-\left(\frac{\partial\mathbf{u}}{\partial\xi_1}\right)^{①}\right]\cos\alpha \tag{33}$$

Substituting Eqs. (26), (27) and (33) into Eq. (22) yields

$$I^{*}_{interface}=0 \tag{34}$$

Similarly, the same result will be obtained for the crack faces penetrated by the interface.

3.3. Discussion on the interaction integral

Substituting Eq. (34) into Eq. (17), the same expression as Eq. (12) is obtained. It implies that Eq. (12) is still valid for nonhomogeneous materials with discontinuous properties (or material interfaces). Namely, the interaction integral method does not require the material to be continuous and hence, its applicable range is greatly enlarged. Moreover, compared with the previous forms, the expression in Eq. (12) can facilitate the numerical implementation for the materials with complicated material interfaces around the crack tip since the integral domain can be chosen arbitrarily.

If the crack face in the integral domain A is curved as shown in Fig. 3(b), the interaction integral can be written as

$$\begin{aligned}I=&\int_A\left(\sigma^{aux}_{ij}u_{j,1}+\sigma_{ij}u^{aux}_{j,1}-\sigma^{aux}_{jk}\varepsilon_{jk}\delta_{1i}\right)q_{,i}\,dA\\ &+\int_A\sigma_{ij}\left[S^{tip}_{ijkl}-S_{ijkl}(x)\right]\sigma^{aux}_{kl,1}q\,dA+I_{crackface}\end{aligned} \tag{35}$$

where $I_{crackface}$ is a line integral on the crack faces. According to Gosz and Moran (2002), we have

$$I_{crackface}=-\int_{\Gamma_c^+\Gamma_c^-\Gamma_A^+\Gamma_A^-}\left(\sigma^{aux}_{ij}u_{j,1}+\sigma_{ij}u^{aux}_{j,1}-\sigma^{aux}_{jk}\varepsilon_{jk}\delta_{1i}\right)m_iq\,dA \tag{36}$$

where Γ_A^+ is a fictitious crack face tangent to the crack tip and Γ_A^- is its opposite path. Taking into account the boundary conditions on Γ_A^+ and Γ_A^-, Eq. (36) can be simplified as

$$\begin{aligned}I_{crackface}=&\int_{\Gamma_c^+\Gamma_c^-}\left(\sigma^{aux}_{ij}\varepsilon_{ij}m_1-m_i\sigma^{aux}_{ij}u_{j,1}-m_i\sigma_{ij}u^{aux}_{j,1}\right)q\,dA\\ &-\int_{\Gamma_A^+\Gamma_A^-}m_i\sigma_{ij}u^{aux}_{j,1}q\,dA\end{aligned} \tag{37}$$

In Eq. (37), if the traction of the actual field is free on Γ_c^+ and Γ_c^-, $m_i\sigma_{ij}u^{aux}_{j,1}=0$.

It is necessary to point out that the present implementation of the interaction integral is invalid when the crack tip is just on the interface or very close to it. If the crack tip is just on the interface or very close to it, the stresses lose the inverse square root singularity and behave like (Hutchinson and Suo, 1992)

$$\sigma_{ij}\sim\overline{K}r^{-s}f_{ij}(\theta) \tag{38}$$

where the factor $\overline{K}$ plays a part analogous to the regular SIF and $f_{ij}(\theta)$ are dimensionless angular distributions. The singularity exponent s ($0<s<1$) depends on material elastic mismatch. If define R_δ to be the ratio of the distance from crack tip to the interface to the crack length, according to many articles (Erdogan et al., 1974 and Wang and Chau, 2001), the inverse square root singularity is still valid for the ratio $R_\delta\geqslant 0.03$ when the crack tip approaches a rigid inclusion. In general, the ratio R_δ can be smaller than 0.03 when the material elastic mismatch is not very large.

4. Extraction of the mixed-mode SIFs

For isotropic materials, the relationship between the J-integral and SIFs is

$$J=\frac{1}{E'_{tip}}\left(K_I^2+K_{II}^2\right) \tag{39}$$

where $E'_{tip}=E_{tip}$ for generalized plane stress and $E'_{tip}=E_{tip}/\left(1-v_{tip}^2\right)$ for plane strain. Here, E_{tip} and v_{tip} are the Young's modulus and the Poisson's ratio at the crack tip. Similarly, the interaction integral can be obtained as (Kim and Paulino, 2003)

$$I=\frac{2}{E'_{tip}}\left(K_IK_I^{aux}+K_{II}K_{II}^{aux}\right) \tag{40}$$

By setting $K_I^{aux}=1, K_{II}^{aux}=0$ and $K_I^{aux}=0, K_{II}^{aux}=1$, mode I and mode II SIFs can be decoupled using Eq. (40).

5. Application of the interaction integral in the XFEM

5.1. Introduction of the XFEM

The extended finite element method (XFEM) was developed by Belytschko and Black (1999) and Moës et al. (1999). It is based on the concept of partition of unity given by Babuška and Melenk (1997) who introduced the local enrichment functions into standard displacement-based approximation to characterize the local features. Therefore, the XFEM allows the discontinuous boundaries, such as cracks or material interfaces, to be independent of the mesh.

In order to describe the discontinuous interfaces, the following signed distance function (Belytschko et al., 2001) is introduced by

$$f_\alpha(\mathbf{x})=\min_{\bar{\mathbf{x}}\in\Gamma_\alpha}\|\mathbf{x}-\bar{\mathbf{x}}\|\text{sign}(\mathbf{n}^+\cdot(\bar{\mathbf{x}}-\mathbf{x})) \tag{41}$$

where $\mathbf{x}$ is a point in the domain Ω; $\bar{\mathbf{x}}$ is a point on the discontinuous surface Γ_α; Γ_α is Γ_c or Γ_p; $\mathbf{n}^+$ is an unit outward normal vector to the surface as shown in Fig. 4. According to the signed distance function (Eq. (41)), we adopt the approximation of the displacement $\mathbf{u}(\mathbf{x})$ as

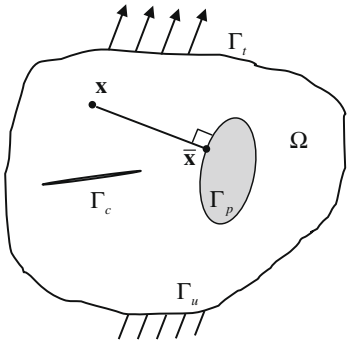

Fig. 4. Illustration of different discontinuous interfaces in a domain Ω.

$$\mathbf{u}^h(\mathbf{x}) = \sum_{I\in D_0} N_I(\mathbf{x})\mathbf{u}_I + \sum_{J\in D_1} N_J(\mathbf{x})\mathbf{b}_J\varphi_J(\mathbf{x}) + \sum_{K\in D_2} N_K(\mathbf{x})\mathbf{c}_K\psi_K(\mathbf{x})$$
$$\varphi_J(\mathbf{x}) = |f_\alpha(\mathbf{x})| - |f_\alpha(\mathbf{x}_J)|, \quad \psi_K(\mathbf{x}) = H(f_\alpha(\mathbf{x})) - H(f_\alpha(\mathbf{x}_K)) \tag{42}$$

Here $N_I(\mathbf{x})$ is the standard finite element shape function; $\varphi_J(\mathbf{x})$ and $\psi_K(\mathbf{x})$ are the shifted enrichment functions for material interfaces and cracks, respectively; $\mathbf{u}_I$ is the nodal displacement; D_0 is the set of all nodes in mesh; D_1 and D_2 are the sets of the nodes enriched with $\varphi_J(\mathbf{x})$ and $\psi_K(\mathbf{x})$, respectively; $\mathbf{b}_J$ and $\mathbf{c}_K$ are the additional degrees of freedom for the nodes in D_1 and D_2, respectively. More details can be found in Belytschko et al. (2001) and Zi and Belytschko (2003) and of course, there are some other choices for the enrichment functions (Moës et al., 2003; Menouillard et al., 2006). In order to improve the numerical precision, the mesh around the crack tip is refined as shown in Fig. 5(a).

Compared with the XFEM using near-tip functions, the present XFEM does not need to obtain the near-tip functions by analytical approach. Thus, the method can easily be applied to the problems in which the analytical expressions of crack-tip fields are difficult to obtain.

5.2. Numerical discretization of the interaction integral

In order to employ the interaction integral method in the XFEM, Eq. (12) should be discretized as

$$I = \sum_{e=1}^{e_A}\sum_{p=1}^{p_e}\left\{(\sigma_{ij}^{aux}u_{j,1} + \sigma_{ij}u_{j,1}^{aux} - \sigma_{jk}^{aux}\varepsilon_{jk}\delta_{1i})q_{,i} + \sigma_{ij}\left[S_{ijkl}^{tip} - S_{ijkl}(x)\right]\sigma_{kl,1}^{aux}q\right\}_p |\mathbf{J}|_p w_p \tag{43}$$

Here, e_A is the number of elements in the integral domain A; p_e is the number of integration points in one element; $|\mathbf{J}|_p$ represents the determinant of Jacobian matrix; w_p is the corresponding weight factor at the integration point p. The derivatives of the actual displacements can be obtained from Eq. (42)

$$u_{i,1} = \sum_{I\in D_0} u_{Ii}N_{I,1} + \sum_{J\in D_1} b_{Ji}(N_{J,1}\varphi_J + N_J\varphi_{J,1}) + \sum_{K\in D_2} c_{Ki}N_{K,1}\psi_K \tag{44}$$

Since ψ_K are constants for all integration points and hence, $\psi_{K,1} = 0$.

For nonhomogeneous materials, actual material properties at integration points are adopted when the element stiffness matrix is formed (Yu et al., 2007). For all examples in this paper, we use 3×3 Gauss quadrature for the standard elements. For elements cut by the crack, we use the technique (Moës et al., 1999) which consists of separately integrating on each side of the crack using a decomposition of the elements into sub-triangles. Four-point integration rule is adopted on each sub-triangle. For the elements containing discontinuous material interfaces, we employ the integration strategy given by Elguedj et al. (2006): each element is divided into 3×3 sub-domains and 3×3 Gauss quadrature is used in each sub-domain. Thus, there are 81 integration points in one of such elements. Fig. 5(b) shows the integration points for different elements.

6. Numerical examples and discussions

In order to demonstrate the accuracy of the numerical technique and verify the convergence of the XFEM and the interaction integral method, we will first present several numerical examples. Then, our attention will be focused on the influences of the material continuity on the mixed-mode SIFs.

6.1. Verification of the numerical method

The interaction integral method combined with the XFEM given in the above section is applied to solve two fracture problems for the materials with continuous nonhomogeneous properties and discontinuous properties, respectively. The results are compared with those from published articles to verify the accuracy of the method.

6.1.1. Example 1: mixed-mode crack problem for nonhomogeneous materials with continuous properties

A two-dimensional functionally graded plate with length L and width W is shown in Fig. 6(a) containing an interior inclined crack

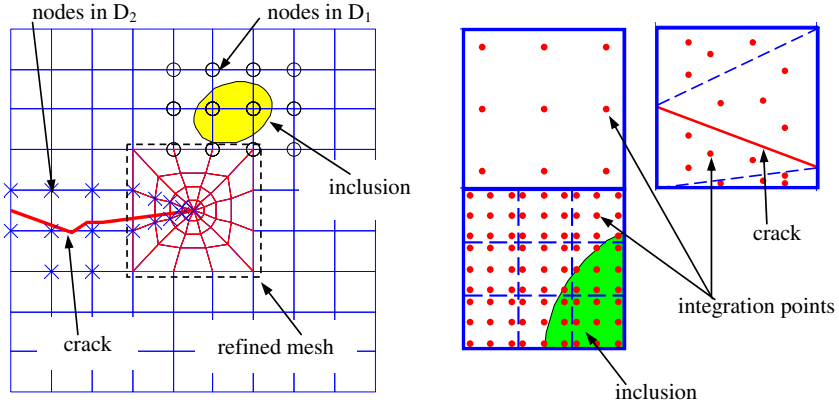

Fig. 5. An edge crack and an elliptical inclusion placed on a mesh: (a) finite element mesh and refined mesh around crack tip; (b) distribution of integration points.

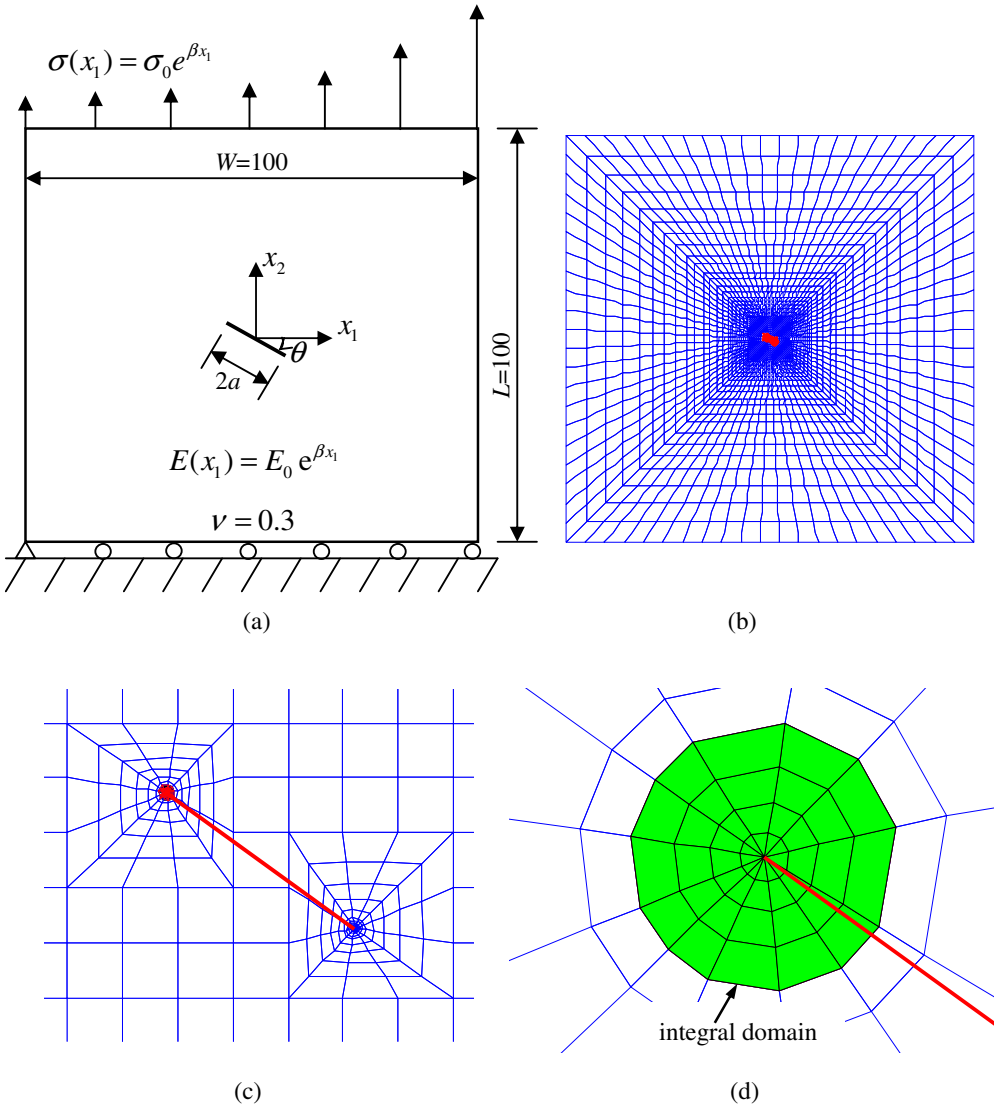

Fig. 6. A nonhomogeneous material plate with an inclined crack: (a) geometry and boundary conditions; (b) complete finite element mesh; (c) refined mesh around crack tips; (d) integral domain to compute the interaction integral.

of length $2a$ and angle θ measured clockwise. The problem of an infinite plate with such a configuration was investigated by Konda and Erdogan (1994). For all examples in this paper, the tension load $\sigma(x_1)$ is applied along the top edge of the plate and the displacement boundary conditions are prescribed such that $u_2 = 0$ along the bottom edge and $u_1 = 0$ for the node at the left-hand side. The Young's modulus is an exponential function of x_1 and the Poisson's ratio ν is constant. The following data are used for numerical analysis: $L = W = 100$; $a/W = 0.01$; $E(x_1) = E_0 e^{\beta x_1}$; $\beta = 0.25$; $E_0 = E(x_1 = 0) = 1$; $\nu = 0.3$; $\sigma(x_1) = \sigma_0 e^{\beta x_1}$; $\sigma_0 = \sigma(x_1 = 0) = 1$; $\theta/\pi = (0, 0.1, 0.2, 0.3, 0.4, 0.5)$; generalized plane stress.

Fig. 6(b) and (c) shows the mesh configuration. Eight-node quadrilateral (Q8) elements are used over most of the mesh. Since the stress field exhibits an inverse square root singularity in this problem, six-node quarter-point (T6qp) singular elements are employed to improve the accuracy. The mesh consists of 2337 Q8 and 24 T6qp elements, with a total of 2361 elements and 7122 nodes. Without special statement, in this paper, four-layer elements

Table 1
Normalized SIFs for a plate with an inclined crack under tension (Example 1: $E(x_1) = E_0 e^{\beta x_1}$, $\beta = 0.25$, $\nu = 0.3$, $\sigma_{22}(x_1) = \sigma_0 e^{\beta x_1}$, $K_0 = \sigma_0\sqrt{\pi a}$).

θ/π	Present results ($a/W = 0.01$)				Konda and Erdogan (1994) ($a/W \to 0$)			
	$K_I(-a)/K_0$	$K_{II}(-a)/K_0$	$K_I(a)/K_0$	$K_{II}(a)/K_0$	$K_I(-a)/K_0$	$K_{II}(-a)/K_0$	$K_I(a)/K_0$	$K_{II}(a)/K_0$
0	0.8186	0	1.1928	0	0.825	0	1.196	0
0.1	0.7444	−0.2523	1.0776	−0.3208	0.750	−0.254	1.081	−0.321
0.2	0.5444	−0.4199	0.7769	−0.5152	0.548	−0.422	0.781	−0.514
0.3	0.2893	−0.4347	0.4123	−0.5042	0.290	−0.437	0.414	−0.504
0.4	0.0743	−0.2805	0.1192	−0.3033	0.075	−0.282	0.121	−0.304
0.5	0	0	0	0	0	0	0	0

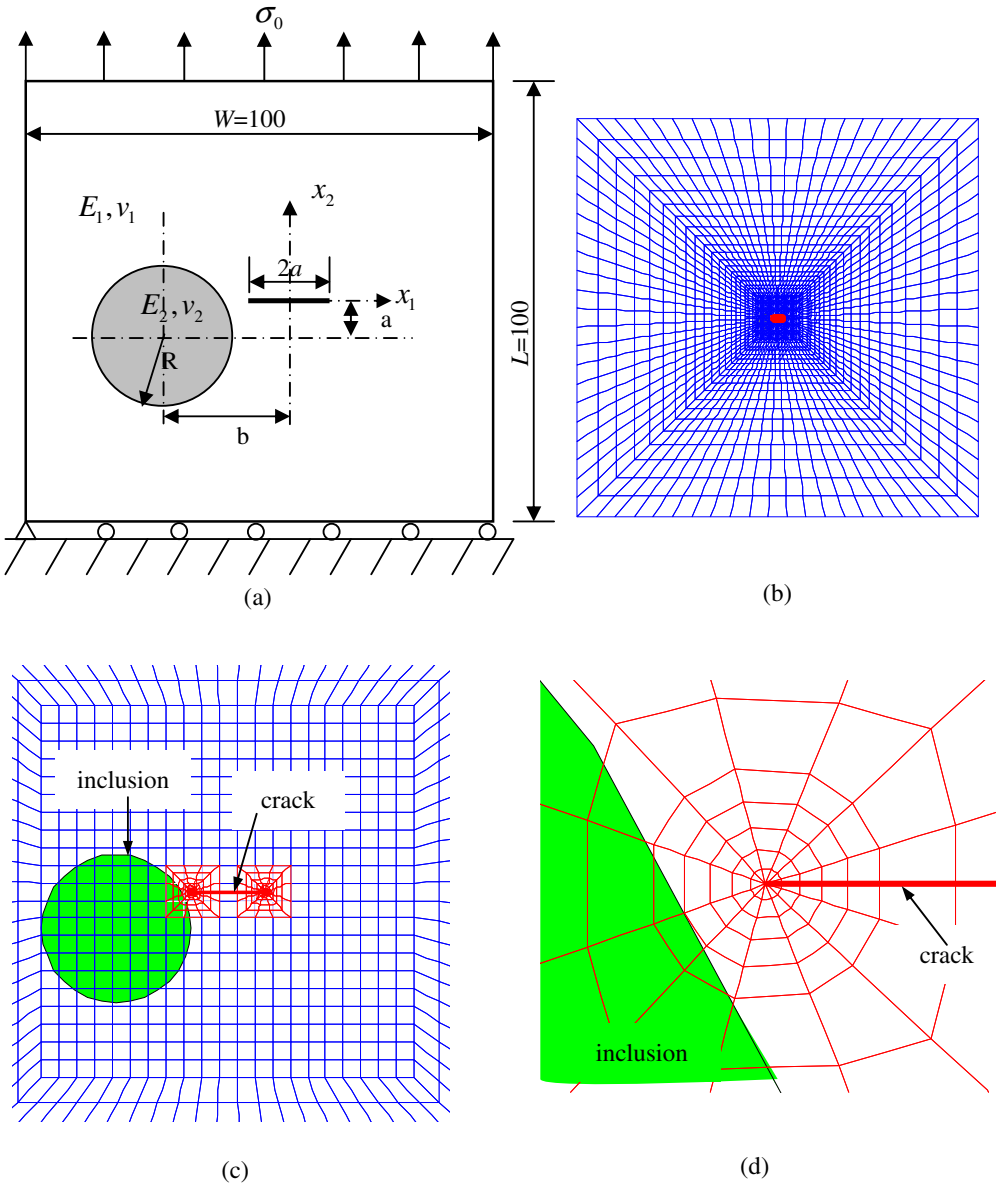

Fig. 7. A plate with a horizontal crack in the neighborhood of a circular rigid inclusion subjected to far field tension: (a) geometry and boundary conditions; (b) complete finite element mesh; (c) the mesh around crack and inclusion; (d) the mesh around the left crack tip.

around the crack tip are adopted for the calculation of the interaction integral as shown in Fig. 6(d). The SIFs are normalized by $K_0 = \sigma_0\sqrt{\pi a}$.

The comparison between the normalized SIFs computed by Eq. (12) and the analytical solution from Konda and Erdogan (1994) is shown in Table 1. It can be found that the relative errors for all SIFs are within 1.5%. Excellent agreement demonstrates that the present method is valid for the fracture problem of nonhomogeneous materials with continuous properties.

6.1.2. Example 2: the fracture problem for materials with discontinuous properties

Fig. 7(a) shows a two-dimensional plate of length L and width W with a horizontal crack of length $2a$ in the neighborhood of a circular inclusion of radius R. The problem of an infinite plate with such a configuration was investigated by Wang and Chau (2001). The inclusion is offset by a distance of b horizontally and c vertically from the origin which coincides with the center of the crack. E_1 and E_2 are the Young's moduli of the matrix and the inclusion, and v_1 and v_2 are the corresponding Poisson's ratios, respectively. The following data are used for numerical analysis: $L = W = 100$; $a/W = 0.01$; $b/a = (2.8, 3, 4, 6, 8, 10)$; $R = 2a$; $E_1 = 1$; $E_2/E_1 = 10^4$; $v_1 = v_2 = 0.35$; $\sigma(x_1) = \sigma_0 = 1$; $K_0 = \sigma_0\sqrt{\pi a}$; generalized plane strain. The mesh configurations are shown in Fig. 7(b)–(d). The mesh consists of 2337 Q8 and 24 T6qp elements with a total of 2361 elements and 7122 nodes.

The comparison between the normalized SIFs and those reported by Wang and Chau (2001) is given in Table 2. It can be observed that the relative errors of the mode I SIFs are all within 2% compared with those of Wang and Chau (2001). Compared with the mode I SIFs, the mode II ones are very small and especially, the mode II ones can be omitted when $b/a = 10$. The relative errors of the mode II SIFs are all within 6% except for $b/a = 10$. That means the interaction integral method is valid for the materials with discontinuous properties.

Table 2
Normalized SIFs for a plate with a crack and an inclusion under far field tension σ_0 (Example 2: $a/W = 0.01$, $R = 2a$, $K_0 = \sigma_0\sqrt{\pi a}$).

b/a	Present results ($E_2/E_1 = 10000, \nu = 3.5$)				Wang and Chau (2001) ($E_2/E_1 = \infty, \nu = 3.5$)			
	$K_I(-a)/K_0$	$K_{II}(-a)/K_0$	$K_I(a)/K_0$	$K_{II}(a)/K_0$	$K_I(-a)/K_0$	$K_{II}(-a)/K_0$	$K_I(a)/K_0$	$K_{II}(a)K_0$
2.8	0.4688	0.1794	0.7641	−0.0668	0.4603	0.1718	0.7626	−0.0708
3.0	0.5908	0.0652	0.8011	−0.0711	0.5810	0.0636	0.7995	−0.0733
4.0	0.8174	−0.0671	0.9065	−0.0568	0.8199	−0.0661	0.9068	−0.0560
6.0	0.9505	−0.0373	0.9687	−0.0255	0.9506	−0.0368	0.9684	−0.0252
8.0	0.9785	−0.0179	0.9844	−0.0129	0.9787	−0.0173	0.9842	−0.0125
10	0.9877	−0.0101	0.9903	−0.0076	0.9878	−0.0091	0.9901	−0.0069

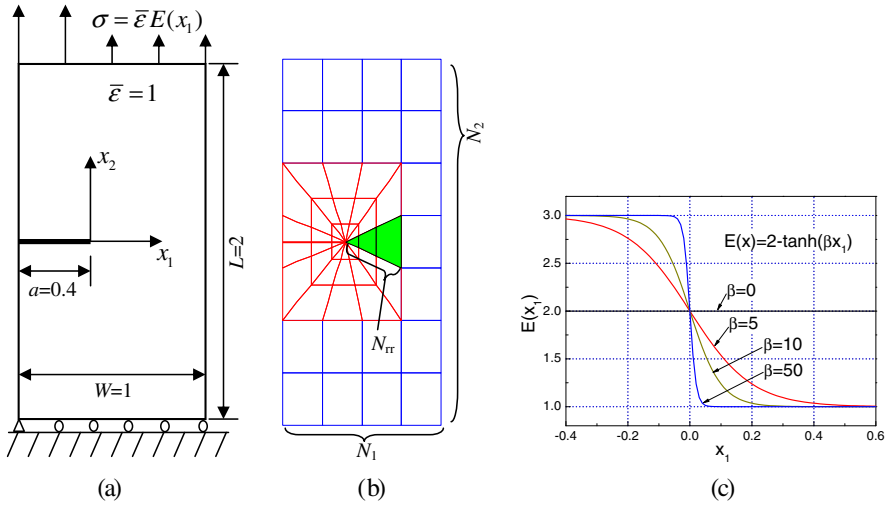

Fig. 8. A nonhomogeneous plate with an edge crack of length a under tension load: (a) geometry and boundary conditions; (b) finite element mesh; (c) Young's modulus.

6.2. The convergence of the XFEM and the interaction integral

In order to verify the present method, some examples are given to verify the convergence.

6.2.1. Example 3: the convergence of the XFEM

Fig. 8(a) shows a nonhomogeneous plate of length L and width W with an edge crack of length a and Fig. 8(b) shows the corresponding mesh configuration. The same problem has been investigated by Eischen (1987) and Menouillard et al. (2006). As shown in Fig. 8(c), The Young's modulus varies as a hyperbolic tangent function of the coordinate x_1. The following data are used for numerical analysis: $L = 2$; $W = 1$; $a/W = 0.4$; $E(x_1) = E_0 - \tanh(\beta x_1)$; $E_0 = 2$; $\beta = (0, 5, 10, 50)$; $\nu = 0.3$; $\sigma = \bar{\varepsilon}E(x_1)$; $\bar{\varepsilon} = 1$; $K_0 = \bar{\varepsilon}E(-0.4)\sqrt{\pi a}$; generalized plane strain.

As shown in Fig. 8(b), N_{rr} denotes the element number in each wedge-shaped domain around the crack tip, and N_1 and N_2 denote the element numbers in x_1 direction and x_2 direction, respectively. Two cases will be discussed.

First, let us keep $N_{rr} = 10$ and consider the variation of total element number $N_1 \times N_2$. Take $N_1 \times N_2$ to be 4×7, 8×15, 16×31, 32×63 and 64×127, sequentially. The convergence of the interaction integral will be examined in the following part and here, four-layer elements around the crack tip are still adopted to be the integral domain.

Table 3 lists the normalized SIFs K_I/K_0 for different $N_1 \times N_2$. The results show that the SIFs nearly have no variation when $N_1 \times N_2$ increase from 32×63 to 64×127 and the variations of the SIFs are all within ±0.05% for all the values of β. For each β, the SIF converges towards a stable value which is just between that obtained by Eischen (1987) and that given by Menouillard et al. (2006). Moreover, the relative errors of the SIFs for different β are all less than 0.5% when the present results are compared with those given by Eischen (1987) and Menouillard et al. (2006).

Second, Let us keep $N_1 \times N_2 = 32 \times 63$ and consider the variation of N_{rr}. Let N_{rr} change from 1 to 12 to test the convergence. The domain to compute interaction integral consists of two-layer elements around the refined mesh and all elements in it. As shown in Fig. 9, the results show that as N_{rr} increases, the SIF corresponding to each β converges towards a stable value which is just between those given by Eischen (1987) and Menouillard et al. (2006) and the differences are extremely small (all within

Table 3
Normalized SIFs K_I/K_0 for a plate with an edge crack under tension (Example 3: $a/W = 0.4$, $E(x_1) = 2 - \tanh(\beta x_1)$, $\nu = 0.3$, $\sigma(x_1) = \bar{\varepsilon}E(x_1)$, $K_0 = \bar{\varepsilon}E(-0.4)\sqrt{\pi a}$, $\bar{\varepsilon} = 1$).

β	Present results (K_I/K_0 for mesh $N_1 \times N_2$)					Eischen (1987)	Menouillard et al. (2006)
	4×7	8×15	16×31	32×63	64×127		
0	2.1228	2.1196	2.1152	2.1117	2.1121	2.112	2.1118
5	2.3139	2.3076	2.3010	2.2963	2.2963	2.295	2.300
10	2.5976	2.5879	2.5793	2.5734	2.5733	2.571	2.586
50	3.3409	3.2535	3.2316	3.2214	3.2198	3.228	3.207

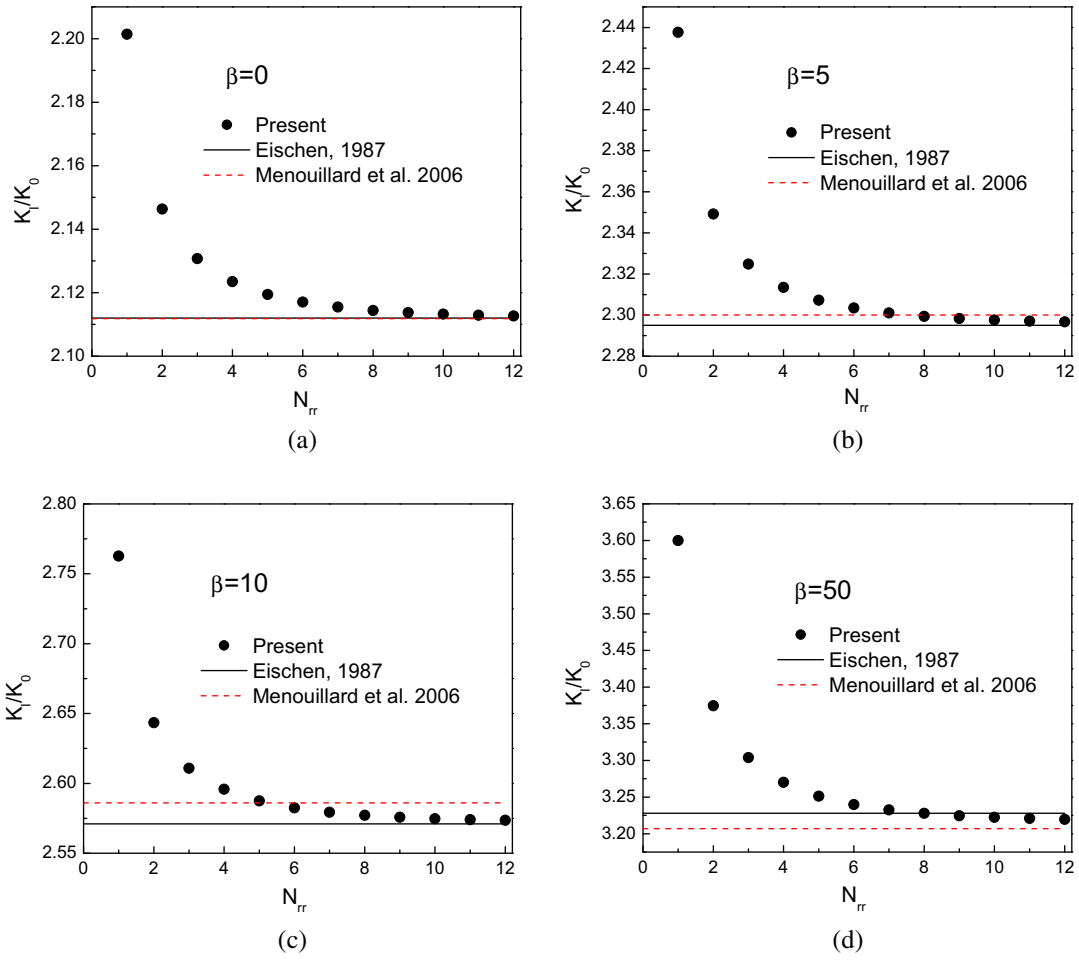

Fig. 9. Normalized SIFs K_I/K_0 for different refined mesh: (a) $\beta = 0$; (b) $\beta = 5$; (c) $\beta = 10$; (d) $\beta = 50$.

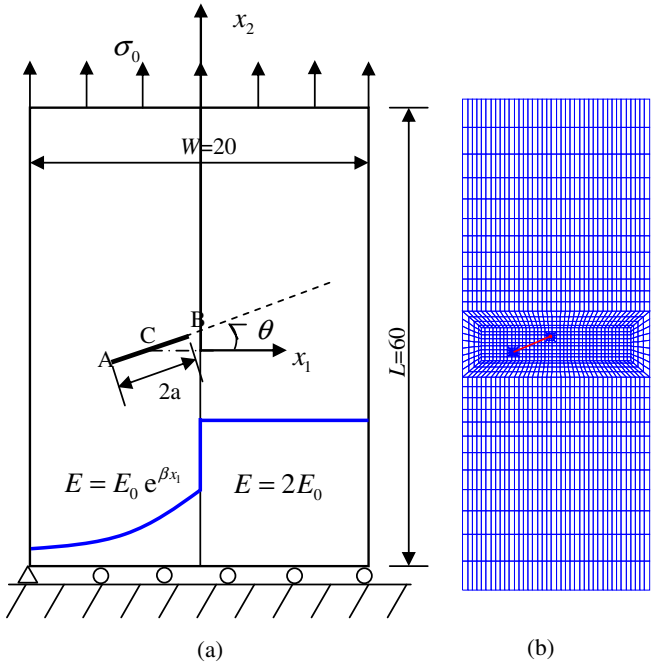

Fig. 10. A nonhomogeneous material plate with a rectilinear crack AB: (a) geometry and boundary conditions; (b) finite element mesh.

±0.08%) when $N_{rr} \geqslant 10$. It implies that the present method is able to obtain stable and accurate results. Moreover, in present range of β, it is enough to obtain convergent results when $N_{rr} = 10$. Therefore, N_{rr} is chosen to be 10 for all examples in this paper.

6.2.2. Example 4: the convergence of the interaction integral

Fig. 10(a) shows a nonhomogeneous plate with an inclined crack of length $2a$ and Fig. 10(b) shows the corresponding mesh configuration. In the plate, there is a bimaterial interface at $x_1 = 0$ and the Young's modulus is defined as

$$E(x_1) = \begin{cases} E_0 e^{\beta x_1} & (x_1 \leqslant 0) \\ 2E_0 & (x_1 > 0) \end{cases} \tag{45}$$

In Eq. (45), E_0 is the modulus value at $x_1 = 0$. Before discussing, we define H_{tip} to be the radial edge length of the elements at the crack tip and R_I to be the radius of the referenced circular contour C_I by which the integral domain is determined as shown in Fig. 11(a). In detail, the integral domain consists of the elements cut by C_I and the elements surrounded by C_I. Eight domains ($R_I/H_{tip} = 3 \times (1, 2, 2^2, 2^3, 2^4, 2^5, 2^6, 2^7)$) are selected to verify the convergence of the SIFs and for simplicity, only four of them are shown in Fig. 11(a)–(d). Two cracks are investigated with crack tips located at $A(-4.6, -1), B(-0.6, 1)$ and $A(-3.4, -1), B(0.6, 1)$, respectively. The following data are used for numerical analysis: $L = 60$; $W = 20$; $E_0 = 1$; $\beta = \ln(10)/W$; $\nu = 0.3$; $\sigma(x_1) = \sigma_0 = 1$; $K_0 = \sigma_0\sqrt{\pi a}$; generalized plane strain. The mesh consists of 1969 Q8 and 24 T6qp elements, with a total of 1993 elements and 6082 nodes.

Table 4 lists the normalized SIFs. It can be seen that the relative error is about 0.1% between the maximal and minimal mode I SIFs and 0.15% for the corresponding mode II SIFs. The results show that the interaction integral exhibits excellent convergence. Therefore, the interaction integral method is reliable for the material with nonhomogeneous and discontinuous properties.

6.3. Influences of the material continuity on the SIFs

In this part, the influences of the material continuity on the SIFs will be investigated by selecting four types of mechanical properties. The model shown in Fig. 10(a) is still adopted. The crack center is located at $C(c,0)$.

According to the continuity of mechanical properties and their derivatives, we select four types of material properties as shown in Fig. 12.

Case 1: The mechanical properties are discontinuous at $x_1 = 0$. The Young's modulus is defined in Eq. (45).

Table 4
Normalized SIFs at crack tip B for different integral domains (Example 4).

Domain	R_I/H_{tip}	$A(-4.6,-1)$, $B(-0.6,1)$		$A(-3.4,-1)$, $B(0.6,1)$	
		$K_I(B)/K_0$	$K_{II}(B)/K_0$	$K_I(B)/K_0$	$K_{II}(B)/K_0$
1	3	0.86436	0.36487	1.58570	0.63464
2	$3*2$	0.86405	0.36470	1.58514	0.63435
3	$3*2^2$	0.86428	0.36456	1.58557	0.63408
4	$3*2^3$	0.86500	0.36467	1.58684	0.63428
5	$3*2^4$	0.86421	0.36481	1.58568	0.63467
6	$3*2^5$	0.86455	0.36437	1.58600	0.63373
7	$3*2^6$	0.86448	0.36455	1.58591	0.63404
8	$3*2^7$	0.86446	0.36453	1.58590	0.63403

Case 2: The mechanical properties are continuous at $x_1 = 0$, but their derivatives are discontinuous. The Young's modulus is defined as

$$E(x_1) = \begin{cases} E_0 e^{\beta x_1} & (x_1 \leqslant 0) \\ E_0 & (x_1 > 0) \end{cases} \tag{46}$$

Here, it should be noted that the Young's modulus at the right side of the plate is the constant term truncated from Taylor series of that at the left side of the plate.

Case 3: The mechanical properties and their first-order derivatives are continuous at $x_1 = 0$, but their high-order derivatives are discontinuous. The Young's modulus is defined as

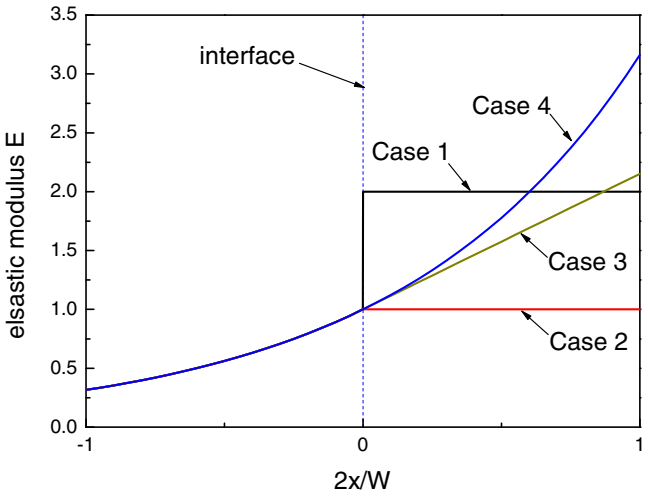

Fig. 12. Four types of material properties with different moduli.

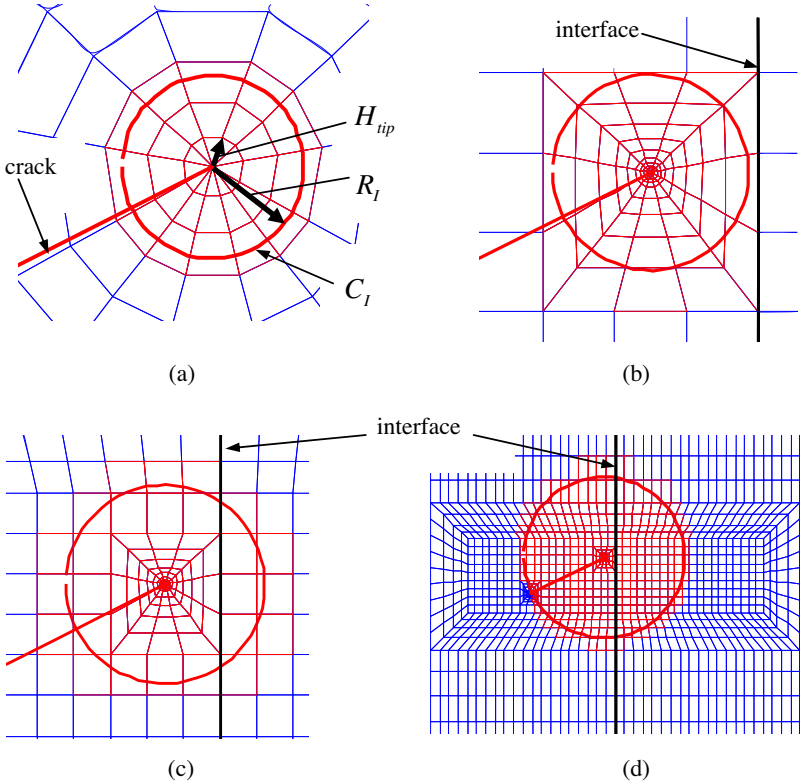

Fig. 11. Different integral domains surrounding the crack tip $B(-0.6,1)$: (a) $R_I/H_{tip} = 3$; (b) $R_I/H_{tip} = 3 \times 2^4$; (c) $R_I/H_{tip} = 3 \times 2^5$; (d) $R_I/H_{tip} = 3 \times 2^7$.

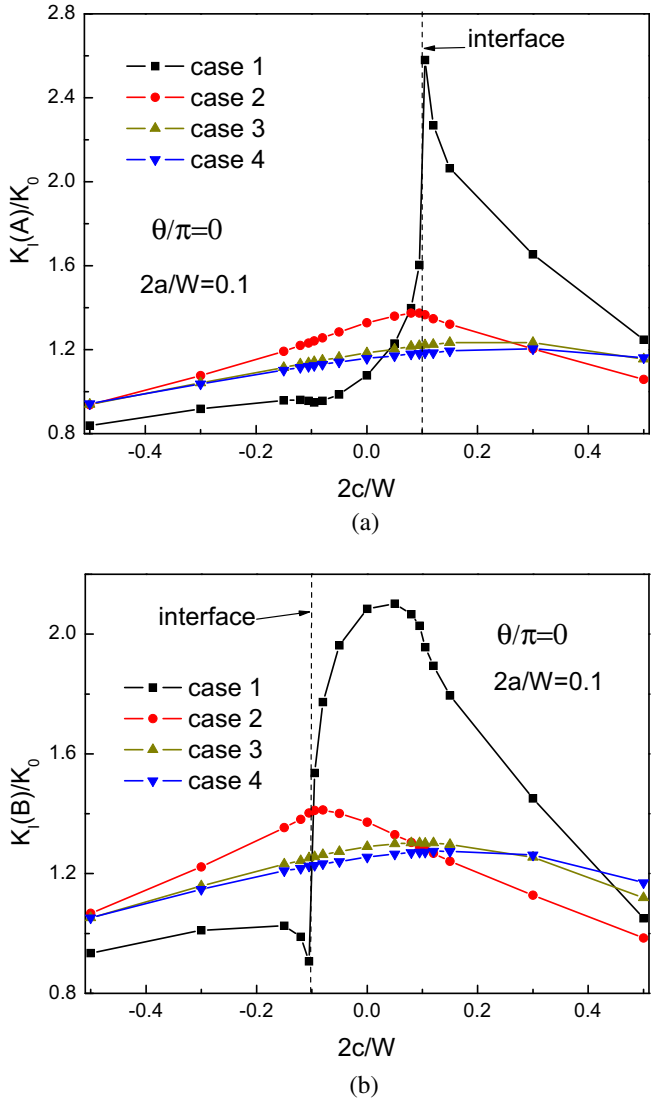

Fig. 13. Normalized mode-I SIFs vary with crack center $2c/W$ for four types of material properties when $2a/W = 0.1$ and $\theta/\pi = 0$: (a) at crack tip A; (b) at crack tip B.

$$E(x_1) = \begin{cases} E_0 e^{\beta x_1} & (x_1 \leqslant 0) \\ E_0(1+\beta x_1) & (x_1 > 0) \end{cases} \tag{47}$$

Here, the Young's modulus at the right side of the plate is the first-order polynomial truncated from Taylor series of that at the left side of the plate.

Case 4: The mechanical properties and their derivatives are continuous at $x_1 = 0$. The Young's modulus is defined as

$$E(x_1) = E_0 e^{\beta x_1} \tag{48}$$

For all the cases, the Poisson's ratio is constant. The following data are used for numerical analysis: $L = 60$; $W = 20$; $\theta/\pi = (0,1/6,1/3)$; $E_0 = 1$; $\beta = \ln(10)/W$; $\nu = 0.3$; $\sigma_0 = 1$; $K_0 = \sigma_0\sqrt{\pi a}$; generalized plane strain.

According to Swenson and Rau (1970), when the crack tip B (A) terminates at the bimaterial interface, the stress singularity exponent s in Eq. (38) is 0.4338 (0.5745) for Case 1. Although the material elastic mismatch is not too large, we still restrict the distance from the crack tip to the interface to be more than 2.5% of the crack length ($R_\delta \geqslant 0.025$) in numerical calculations.

Fig. 13(a) and (b) shows that the normalized mode-I SIFs vary with crack center coordinate $2c/W$ when $2a/W = 0.1$ and $\theta/\pi = 0$. The range $2c/W$ is from -0.5 to 0.5, which means the crack moves from the center of left half plate to the center of right half plate. For Case 1, it can be found that the normalized SIFs vary with the increasing of $2c/W$ as follows: (1) when $2c/W < -0.1$ and the crack tip B is not very close to the interface, both $K_I(A)/K_0$ and $K_I(B)/K_0$ experience a slight increasing. (2) When the crack tip B is close to the interface, $K_I(A)/K_0$ varies slightly, but $K_I(B)/K_0$ decreases initially to a minimum value when the crack tip B approaches the interface ($2c/W \approx -0.1$) and then, increases quickly after the crack tip B passes the interface. (3) Between $-0.1 \leqslant 2c/W \leqslant 0.1$ in which the crack intersects the interface, the normalized SIFs vary dramatically. It implies the material mismatch can affect the crack tip fields greatly. (4) After the crack tip B passes the interface, $K_I(A)/K_0$ increases very quickly to a peak value when the crack tip A approaches the interface ($2c/W \approx 0.1$). (5) After the crack tip A passes the interface ($2c/W > 0.1$), both A and B lie in the same material and the effect of material mismatch becomes slight so that $K_I(A)/K_0$ and $K_I(B)/K_0$ decrease together. In brief, when the crack tip passes the interface, the SIFs usually have great variations. The similar effects have been found by Erdogan and Gupta (1975) when the crack tip approaches the interface of a circular inclusion.

For Case 2, $K_I(A)/K_0$ ($K_I(B)/K_0$) increases initially with the increasing of $2c/W$, attain its maximum when $2c/W \approx 0.1$ ($2c/W \approx -0.1$) and then, decreases with $2c/W$ when $2c/W > 0.1$ ($2c/W > -0.1$). It implies that the SIFs have a kinking behavior at the interface where the first-order derivatives of the mechanical properties are discontinuous. The same phenomenon has been observed by Guo and Noda (2008).

For Case 3 and Case 4, the SIFs vary smoothly and $K_I(A)/K_0$ ($K_I(B)/K_0$) has no kinking behavior at $2c/W \approx 0.1$ ($2c/W \approx -0.1$). In comparison of the two cases, the magnitude and the varying trend of the normalized SIFs are quite similar. Therefore, the continuity of high-order derivatives of mechanical properties affects the SIFs slightly.

From the above four cases, it can be found that the improvement of the continuity of material properties can reduce the varying range of the SIFs and smooth their varying trends, especially for Case 1 and Case 2. The larger the elastic modulus is in right half plate, the smaller the SIFs are in left half plate. Therefore, the SIFs for Case 3 and Case 4 are bigger than those for case 1 and smaller than those for Case 2 in left half plate.

Figs. 14 and 15 show the mixed-mode SIFs variation with $2c/W$ for the slanted angles $\theta/\pi = 1/6$ and $\theta/\pi = 1/3$, respectively. Although there exist some differences in the magnitude of the mode I and II SIFs, their varying trends are the same as those of pure mode I crack shown in Fig. 13(a) and (b). These phenomena indicate that the mode I and II SIFs are affected greatly by the mechanical properties and their first-order derivatives, while the high-order derivatives have slight influence on the SIFs. The similar effect has been observed by Li et al. (2006) for the interface crack.

7. Summary and conclusions

In this paper, a new domain expression of the interaction integral is derived. This expression does not contain any derivatives of material property parameters, and it is still valid even when the integral domain contains material interfaces. The interaction integral method is combined with the XFEM. Several fracture examples are adopted to verify the numerical precision. It is found that the numerical results are in good agreement with those appearing in

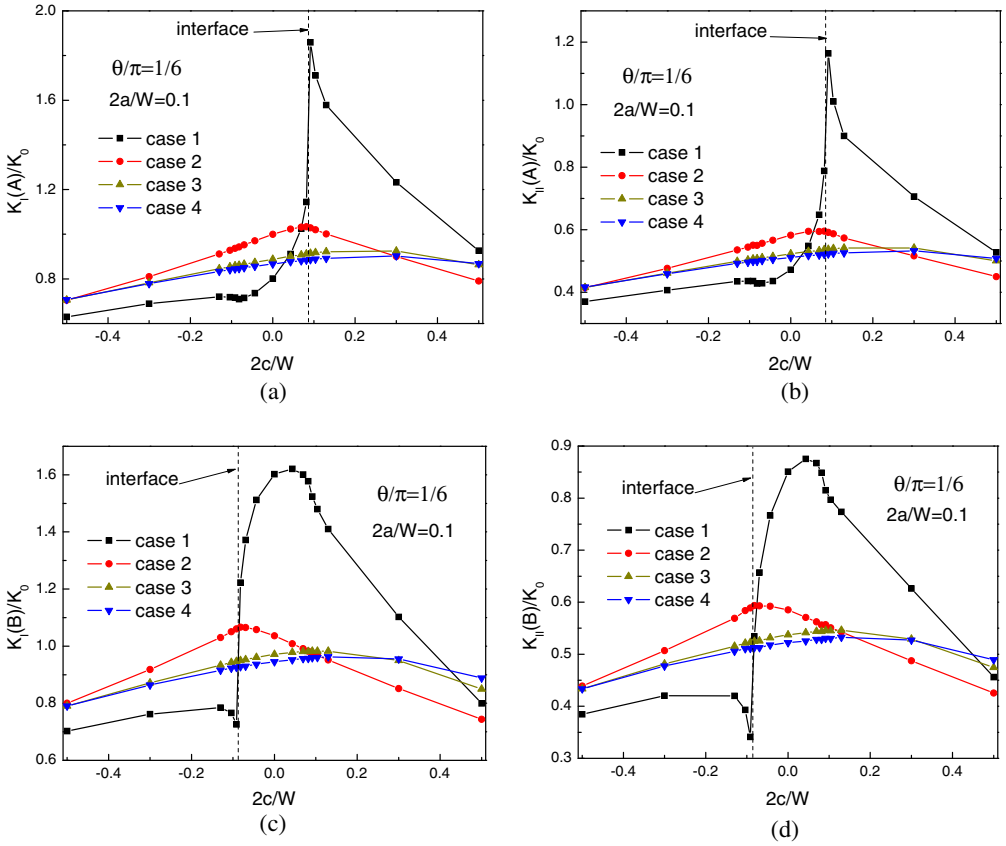

Fig. 14. Normalized SIFs vary with crack center $2c/W$ for four types of material properties when $2a/W = 0.1$ and $\theta/\pi = 1/6$: (a) normalized mode-I SIFs at crack tip A; (b) normalized mode-I SIFs at crack tip B. (c) normalized mode-II SIFs at crack tip A; (d) normalized mode-II SIFs at crack tip B.

published papers. Moreover, the interaction integral method shows good convergence for nonhomogeneous and discontinuous material properties.

In application of the present method, the influences of the material continuity on mixed-mode SIFs are investigated. It can be observed that: (1) The mechanical properties and their first-order derivatives affect the SIFs greatly, while their higher-order derivatives have little influence on the SIFs. (2) When the mechanical properties are discontinuous (Case 1), the SIFs vary dramatically with crack location. (3) When the material properties are continuous but their first-order derivatives are discontinuous (Case 2), the SIFs have a kinking behavior at the interface. (4) Further improvement on the continuity (Case 3 and Case 4) can smooth the variation trends of the SIFs and no kinking behavior is observed at the interface.

Acknowledgement

This work is sponsored by the Program of Excellent Team in Harbin Institute of Technology, NSFC (10432030 and 10872056) and NCET-08-0151.

Appendix A

In the local polar coordinate system shown in Fig. 1, the auxiliary fields can be defined as (Kim and Paulino, 2005)

$$u_i^{aux} = K_I^{aux} f_i^I(r^{1/2}, \theta, \mu_{tip}, \kappa_{tip}) + K_{II}^{aux} f_i^{II}(r^{1/2}, \theta, \mu_{tip}, \kappa_{tip}) \tag{A1}$$

$$\sigma_{ij}^{aux} = K_I^{aux} g_{ij}^I(r^{-1/2}, \theta) + K_{II}^{aux} g_{ij}^{II}(r^{-1/2}, \theta) \tag{A2}$$

$$\varepsilon_{ij}^{aux} = S_{ijkl}(x)\sigma_{kl}^{aux} \quad (i,j,k,l = 1,2) \tag{A3}$$

Here, K_I^{aux} and K_{II}^{aux} are the auxiliary mode I and II SIFs, respectively, and the representative functions f_i^I, f_i^{II}, g_{ij}^I and g_{ij}^{II} are (Williams, 1957)

$$\begin{aligned}
f_1^I &= \frac{1}{2\mu_{tip}}\sqrt{\frac{r}{2\pi}}\cos\frac{\theta}{2}\left(\kappa_{tip} - 1 + 2\sin^2\frac{\theta}{2}\right)\\
f_1^{II} &= \frac{1}{2\mu_{tip}}\sqrt{\frac{r}{2\pi}}\sin\frac{\theta}{2}\left(\kappa_{tip} + 1 + 2\cos^2\frac{\theta}{2}\right)\\
f_2^I &= \frac{1}{2\mu_{tip}}\sqrt{\frac{r}{2\pi}}\sin\frac{\theta}{2}\left(\kappa_{tip} + 1 - 2\cos^2\frac{\theta}{2}\right)\\
f_2^{II} &= -\frac{1}{2\mu_{tip}}\sqrt{\frac{r}{2\pi}}\cos\frac{\theta}{2}\left(\kappa_{tip} - 1 - 2\sin^2\frac{\theta}{2}\right)
\end{aligned} \tag{A4}$$

$$\begin{aligned}
g_{11}^I &= \frac{1}{\sqrt{2\pi r}}\cos\frac{\theta}{2}\left(1 - \sin\frac{\theta}{2}\sin\frac{3\theta}{2}\right)\\
g_{11}^{II} &= -\frac{1}{\sqrt{2\pi r}}\sin\frac{\theta}{2}\left(2 + \cos\frac{\theta}{2}\cos\frac{3\theta}{2}\right)\\
g_{22}^I &= \frac{1}{\sqrt{2\pi r}}\cos\frac{\theta}{2}\left(1 + \sin\frac{\theta}{2}\sin\frac{3\theta}{2}\right)\\
g_{22}^{II} &= \frac{1}{\sqrt{2\pi r}}\sin\frac{\theta}{2}\cos\frac{\theta}{2}\cos\frac{3\theta}{2}\\
g_{12}^I &= g_{21}^I = g_{22}^{II}, \quad g_{12}^{II} = g_{21}^{II} = g_{11}^I
\end{aligned} \tag{A5}$$

Here, $\kappa_{tip} = 3 - 4\nu_{tip}$ for plane strain and $\kappa_{tip} = (3 - \nu_{tip})/(1 + \nu_{tip})$ for plane stress, μ_{tip} and ν_{tip} are the shear modulus and the Poisson's ratio at crack tip location, respectively. It should be noted that except at the crack tip (Kim and Paulino, 2003)

$$\varepsilon_{ij}^{aux} \neq \left(u_{i,j}^{aux} + u_{j,i}^{aux}\right)/2 \tag{A6}$$

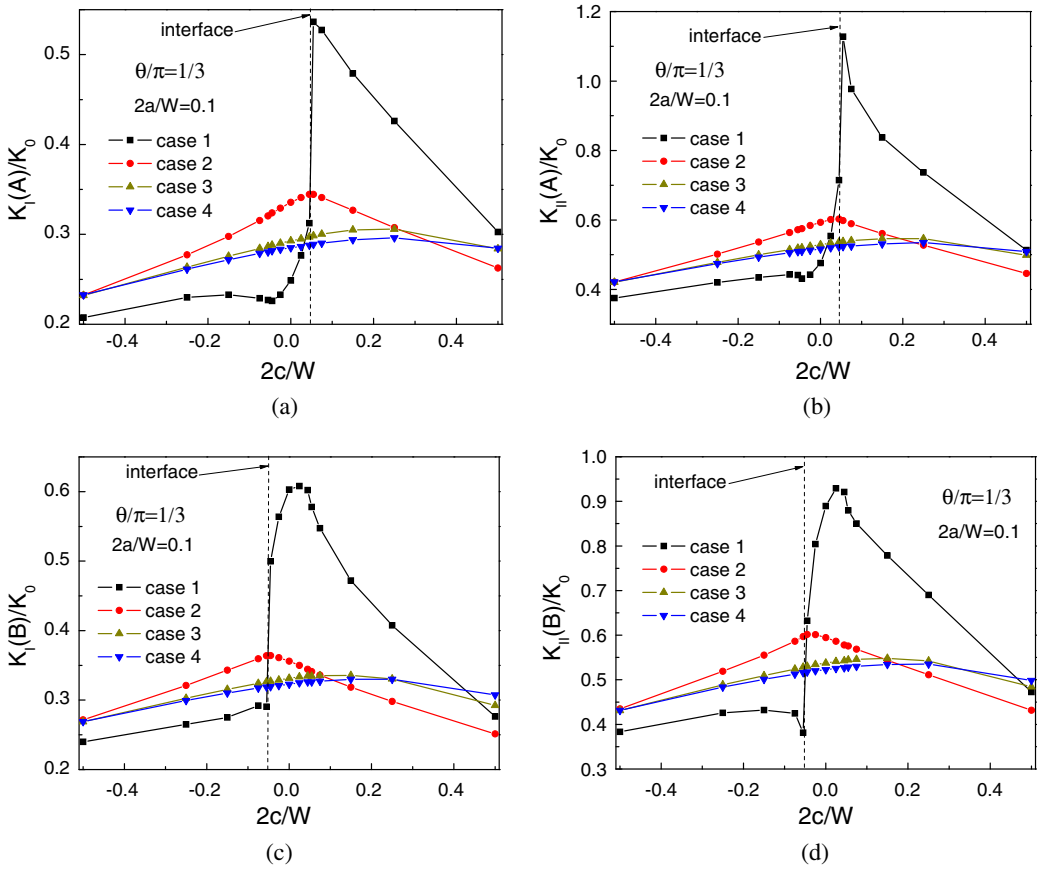

Fig. 15. Normalized SIFs intensity factors vary with crack center $2c/W$ for four types of material properties when $2a/W = 0.1$ and $\theta/\pi = 1/3$: (a) normalized mode-I SIFs at crack tip A; (b) normalized mode-I SIFs at crack tip B. (c) normalized mode-II SIFs at crack tip A; (d) normalized mode-II SIFs at crack tip B.

Appendix B

The details regarding Eq. (32) are as follows

$$
\begin{aligned}
\boldsymbol{\sigma}^{aux} : (\boldsymbol{\varepsilon}^{②} - \boldsymbol{\varepsilon}^{①}) n_1 &= \boldsymbol{\sigma}^{aux} : [(\vec{\nabla}\mathbf{u})^{②} - (\vec{\nabla}\mathbf{u})^{①}] n_1 \\
&= \sigma_{ij}^{aux} \mathbf{e}_i \mathbf{e}_j : \frac{\mathbf{e}_k}{h_{\underline{k}}} \left\{ \left[\frac{\partial (u_l \mathbf{e}_l)}{\partial \xi_k}\right]^{②} - \left[\frac{\partial (u_l \mathbf{e}_l)}{\partial \xi_k}\right]^{①} \right\} n_1 \\
&= \sigma_{ij}^{aux} \mathbf{e}_j \cdot \frac{\delta_{ik}}{h_{\underline{k}}} \left\{ \left[\frac{\partial (u_l \mathbf{e}_l)}{\partial \xi_k}\right]^{②} - \left[\frac{\partial (u_l \mathbf{e}_l)}{\partial \xi_k}\right]^{①} \right\} n_1 \\
&= \sigma_{1j}^{aux} \mathbf{e}_j \cdot \frac{1}{h_1} \left\{ \left[\frac{\partial (u_l \mathbf{e}_l)}{\partial \xi_1}\right]^{②} - \left[\frac{\partial (u_l \mathbf{e}_l)}{\partial \xi_1}\right]^{①} \right\} n_1 \\
&\quad + \sigma_{2j}^{aux} \mathbf{e}_j \cdot \frac{1}{h_2} \left\{ \left[\frac{\partial (u_l \mathbf{e}_l)}{\partial \xi_2}\right]^{②} - \left[\frac{\partial (u_l \mathbf{e}_l)}{\partial \xi_2}\right]^{①} \right\} n_1 \\
&= \mathbf{e}_1 \cdot \boldsymbol{\sigma}^{aux} \cdot \frac{1}{h_1} \left\{ \left[\frac{\partial \mathbf{u}}{\partial \xi_1}\right]^{②} - \left[\frac{\partial \mathbf{u}}{\partial \xi_1}\right]^{①} \right\} n_1 \\
&\quad + \mathbf{e}_2 \cdot \boldsymbol{\sigma}^{aux} \cdot \frac{1}{h_2} \left\{ \left[\frac{\partial \mathbf{u}}{\partial \xi_2}\right]^{②} - \left[\frac{\partial \mathbf{u}}{\partial \xi_2}\right]^{①} \right\} n_1
\end{aligned}
\tag{B1}
$$

Here, the underlined subscript $\underline{k}$ denotes no sum on k.

References

Babuška, I., Melenk, J.M., 1997. The partition of unity method. International Journal for Numerical Methods in Engineering 40, 727–758.

Belytschko, T., Black, T., 1999. Elastic crack growth in finite elements with minimal remeshing. International Journal for Numerical Methods in Engineering 45, 601–620.

Belytschko, T., Moës, N., Usui, S., Parimi, C., 2001. Arbitrary discontinuities in finite elements. International Journal for Numerical Methods in Engineering 50, 993–1013.

Birman, V., Byrd, L.W., 2007. Modeling and analysis of functionally graded materials and structures. Applied Mechanics Reviews 60, 195–216.

Dolbow, J.E., Gosz, M., 2002. On the computation of mixed-mode stress intensity factors in functionally graded materials. International Journal of Solids and Structures 39, 2557–2574.

Eischen, J.W., 1987. Fracture of nonhomogeneous materials. International Journal of Fracture 34, 3–22.

Elguedj, T., Gravouil, A., Combescure, A., 2006. Appropriate extended functions for X-FEM simulation of plastic fracture mechanics. Computer Methods in Applied Mechanics and Engineering 195, 501–515.

Erdogan, F., Gupta, G.D., 1975. The inclusion problem with a crack crossing the boundary. International Journal of Fracture 11, 13–27.

Erdogan, F., Gupta, G.D., Ratwani, M., 1974. Interaction between a circular inclusion and an arbitrarily oriented crack. Journal of Applied Mechanics 47, 1007–1013.

Gosz, M., Moran, B., 2002. An interaction energy integral method for computation of mixed-mode stress intensity factors along non-planar crack fronts in three dimensions. Engineering Fracture Mechanics 69, 299–319.

Gosz, M., Dolbow, J., Moran, B., 1998. Domain integral formulation for stress intensity factor computation along curved three-dimensional interface cracks. International Journal of Solids and Structures 35 (15), 1763–1783.

Guo, L.C., Noda, N., 2008. Fracture mechanics analysis of functionally graded layered structures with a crack crossing the interface. Mechanics of Materials 40, 81–99.

Honein, T., Herrmann, G., 1997. Conservation laws in nonhomogeneous plane elastostatics. Journal of the Mechanics and Physics of Solids 45 (5), 789–805.

Hutchinson, J.W., Suo, Z., 1992. Mixed mode cracking in layered materials. Advances in Applied Mechanics 29, 63–191.

Jin, Z.H., Sun, C.T., 2007. Integral Representation of Energy Release Rate in Graded Materials. Journal of Applied Mechanics 74, 1046–1048.

Johnson, J., Qu, J.M., 2007. An interaction integral method for computing mixed mode stress intensity factors for curved bimaterial interface cracks in non-uniform temperature fields. Engineering Fracture Mechanics 74, 2282–2291.

KC, A., Kim, J.H., 2008. Interaction integrals for thermal fracture of functionally graded materials. Engineering Fracture Mechanics 75, 2542–2565.

Kim, J.H., Paulino, G.H., 2003. T-stress, mixed-mode stress intensity factors, and crack initiation angles in functionally graded materials: a unified approach using the interaction integral method. Computer Methods in Applied Mechanics and Engineering 192, 1463–1494.

Kim, J.H., Paulino, G.H., 2005. Consistent formulations of the interaction integral method for fracture of functionally graded materials. Journal of Applied Mechanics 72, 351–364.
Konda, N., Erdogan, F., 1994. The mixed mode crack problem in a non-homogeneous elastic medium. Engineering Fracture Mechanics 47 (4), 533–545.
Krysl, P., Belytschko, T., 1999. The element free Galerkin method for dynamic propagation of arbitrary 3-D cracks. International Journal for Numerical Methods in Engineering 44, 767–800.
Leggoe, J.W., Hu, X.Z., Bush, M.B., 1996. Crack tip damage development and crack growth resistance in particulate reinforced metal matrix composites. Engineering Fracture Mechanics 53 (6), 873–895.
Li, Y.D., Zhang, H.C., Tan, W., 2006. Fracture analysis of functionally gradient weak/micro-discontinuous interface with finite element method. Computational Materials Science 38, 454–458.
Menouillard, T., Elguedj, T., Combescure, A., 2006. Mixed-mode stress intensity factors for graded materials. International Journal of Solids and Structures 43, 1946–1959.
Moës, N., Dolbow, J., Belytschko, T., 1999. A finite element method for crack growth without remeshing. International Journal for Numerical Methods in Engineering 46, 131–150.
Moës, N., Cloirec, M., Cartraud, P., Remacle, J.F., 2003. A computational approach to handle complex microstructure geometries. Computer Methods in Applied Mechanics and Engineering 192, 3163–3177.
Moran, B., Shih, C.F., 1987a. A general treatment of crack tip contour integrals. International Journal of Fracture 35, 295–310.
Moran, B., Shih, C.F., 1987b. Crack tip and associated domain integrals from momentum and energy balance. Engineering Fracture Mechanics 27 (6), 615–642.
Nahta, R., Moran, B., 1993. Domain integrals for axisymmetric interface crack problems. International Journal of Solids and Structures 30 (15), 2027–2040.
Nakamura, T., 1991. Three-dimensional stress fields of elastic interface cracks. Journal of Applied Mechanics 58, 939–946.
Rahman, S., Chakraborty, A., 2007. A stochastic micromechanical model for elastic properties of functionally graded materials. Mechanics of Materials 39, 548–563.
Rao, B.N., Rahman, S., 2003. An interaction integral method for analysis of cracks in orthotropic functionally graded materials. Computational Mechanics 32, 40–51.
Réthoré, J., Gravouil, A., Morestin, F., Combescure, A., 2005. Estimation of mixed-mode stress intensity factors using digital image correlation and an interaction integral. International Journal of Fracture 132, 65–79.
Rice, J.R., 1968. A path independent integral and the approximate analysis of strain concentration by notches and cracks. Journal of Applied Mechanics 35, 379–386.
Rice, J.R., 1988. Elastic fracture mechanics concepts for interfacial cracks. Journal of Applied Mechanics 55, 98–103.
Smelser, R.E., Gurtin, M.E., 1977. On the *J*-integral for bi-material bodies. International Journal of Fracture 13, 382–384.
Song, S.H., Paulino, G.H., 2006. Dynamic stress intensity factors for homogeneous and smoothly heterogeneous materials using the interaction integral method. International Journal of Solids and Structures 43, 4830–4866.
Stern, M., Becker, E.B., Dunham, R.S., 1976. A contour integral computation of mixed-mode stress intensity factors. International Journal of Fracture 12 (3), 359–368.
Swenson, D.O., Rau, C.A., 1970. The stress distribution around a crack perpendicular to an interface between materials. International Journal of Fracture Mechanics 6 (4), 357–365.
Walters, M.C., Paulino, G.H., Dodds, R.H., 2006. Computation of mixed-mode stress intensity factors for cracks in three-dimensional functionally graded solids. Journal of Engineering Mechanics 132 (1), 1–15.
Wang, Y.B., Chau, K.T., 2001. A new boundary element method for mixed boundary value problems involving cracks and holes: interactions between rigid inclusions and cracks. International Journal of Fracture 110, 387–406.
Wang, S.S., Yau, J.F., Corten, H.T., 1980. A mixed-mode crack analysis of rectilinear anisotropic solids using conservation laws of elasticity. International Journal of Fracture 16 (3), 247–259.
Williams, M.L., 1957. On the stress distribution at the base of a stationary crack. Journal of Applied Mechanics 24 (1), 109–114.
Yang, L.H., Li, Z.H., 2004. The interaction of mode I crack with multi-inclusions in a three-phase model. International Journal of Fracture 127, 193–200.
Yau, J.F., Wang, S.S., Corten, H.T., 1980. A mixed-mode crack analysis of isotropic solids using conservation laws of elasticity. Journal of Applied Mechanics 47 (2), 335–341.
Yu, H.J., Guo, L.C., Wu, L.Z., 2007. Numerical investigation on the fracture behaviors of three-dimensional functionally graded materials. Key Engineering Materials, 1098–1101.
Zi, G., Belytschko, T., 2003. New crack-tip elements for XFEM and applications to cohesive cracks. International Journal for Numerical Methods in Engineering 57, 2221–2240.